RSC Advances

PAPER

View Article Online
View Journal | View Issue

Check for updates

Cite this: *RSC Adv.*, 2022, **12**, 29939

Ni^{II} and Co^{II} binary and ternary complexes of 3-formylchromone: spectroscopic characterization, antimicrobial activities, docking and modeling studies

Noha Nabil, Omima M. I. Adly, Magdy Shebl, Ali Taha and Fatma Samy *

Reactions of 3-formylchromone (L) with Ni(II) and Co(II) ions having different anions (acetate, perchlorate, nitrate, and chloride) yielded a series of binary and ternary octahedral complexes with the general formula $[ML_nL'_mX_y(S)_a]Z_y \cdot bS$, where M = Ni or Co, n = 1–3, L′ = auxiliary ligand = 8-hydroxyquinoline or 1,10-phenanthroline, m = 1 or 2, X = acetate or chloride, y = 0 or 2, S = H_2O or MeOH, a = 0–2, Z = nitrate or perchlorate and b = 0–1.5. Elemental and thermal analyses and infra-red, electronic, mass, magnetic susceptibility and molar conductivity measurements were successfully utilized to characterize the structures of the chromone complexes. The chromone ligand acts as a neutral bidentate ligand through its formyl and γ-pyrone oxygen atoms. The obtained complexes were formed with molar ratios 1 : 2 and 1 : 3 M : L for the binary and 1 : 2 : 1 and 1 : 1 : 1 M : L : L′ for the ternary complexes. The kinetic parameters of the thermal degradation steps were estimated and explained using the Coats–Redfern equations. The synthesized complexes showed antimicrobial activity with higher activity toward *Candida albicans* and *Bacillus subtilis*. Docking studies showed good agreement with the antimicrobial activity. Molecular modeling of the synthesized complexes was performed using Hyperchem at the *PM3* level and the calculated structures correlate with the experimental data.

Received 4th June 2022
Accepted 29th September 2022

DOI: 10.1039/d2ra03475a

rsc.li/rsc-advances

Open Access Article. Published on 19 October 2022. Downloaded on 2/8/2026 7:06:59 AM.
This article is licensed under a Creative Commons Attribution-NonCommercial 3.0 Unported Licence.

1. Introduction

Chromones are important natural compounds with a γ-pyrone heterocyclic ring structure. They are known for inhibiting enzymes, including mushroom tyrosinase and protein kinase-C.[1] Plant leaves and flowers are sources and contain chromone as a pigment. They are essential for the production of various xanthones, transition metal chelates, and heterocyclic compounds with oxygen.[2] The flexible reactive synthon chromone-3-carbaldehyde (3-formychromone) has attracted much attention of late.[3] This molecule can react as an aldehyde, a Michael acceptor, a heterodiene, and a dienophile since it has three highly electrophilic carbons (C-2 and C-4 of the pyrone moiety and the carbon atom of the formyl group).[3] Due to their three electrophilic sites (C1, C3, and C4), 3-formylchromones are versatile, practical, and commercial building blocks that are frequently used in the creation of functionalized fused heterocycles.[4] The two electrophilic sites (C1 and C4) may react with bis-nucleophilic reagents, such as enamine ketones/esters, heterocyclic ketene aminals (HKAs), or 1,1-enediamine (EDAMs)[4] among others,[4] to produce the site-selective synthesis of fused heterocycles. Because it comprises a wide range of pharmacologically active chemicals, such as antimicrobial, anti-inflammatory, antiallergic, anti-HIV, antitumor, antiplaque, antioxidant and neuroprotective,[5–9] as well as acting as a fluorescent marker, the bicyclic chromone moiety has been categorized as a favorable structure in drug discovery.[2] Protein kinases P13Ks, CDK, and TNF signaling, among other cancer targets, are known to be inhibited by chromone derivatives. The chromone derivative LY294002 was discovered to be a kinase inhibitor through inhibiting the phosphatidylinositol-3-kinase (PI3K) signaling pathway.[10] The cyclin-dependent kinase (CDK) inhibitor flavopirid, a different chromen-4-one molecule, was discovered to be capable of inhibiting the cell cycle and inducing apoptosis.[10] Another set of substituted chromones that provided site-specificity for the ABCG2 protein were discovered to be powerful inhibitors of breast cancer strains. The 5-(4-bromobenzyloxy) 2-(2-(5-methoxyindolyl) ethyl-1-carbonyl)-4*H*-chromen-4-one compound in this series showed strong inhibition and minimal toxicity, showing a noticeably high therapeutic profile.[10] There are a few intriguing literature reports on biological investigations, such as the DNA binding and cytotoxicity profile of copper(II)-appended chromone therapeutic candidates that have demonstrated varied responses with diverse cytotoxicity potencies against various phenotypes of malignancies.[10]

Department of Chemistry, Faculty of Education, Ain Shams University, Roxy, Cairo 11566, Egypt. E-mail: noha.nabil1986@yahoo.com; omima_adly@edu.asu.edu.eg; magdyshebl@edu.asu.edu.eg; alitaha@edu.asu.edu.eg; fatmasame@edu.asu.edu.eg; Fax: +20 0222581243; Tel: +20 1096418414

© 2022 The Author(s). Published by the Royal Society of Chemistry

Open Access Article. Published on 19 October 2022. Downloaded on 2/8/2026 7:06:59 AM. This article is licensed under a Creative Commons Attribution-NonCommercial 3.0 Unported Licence.

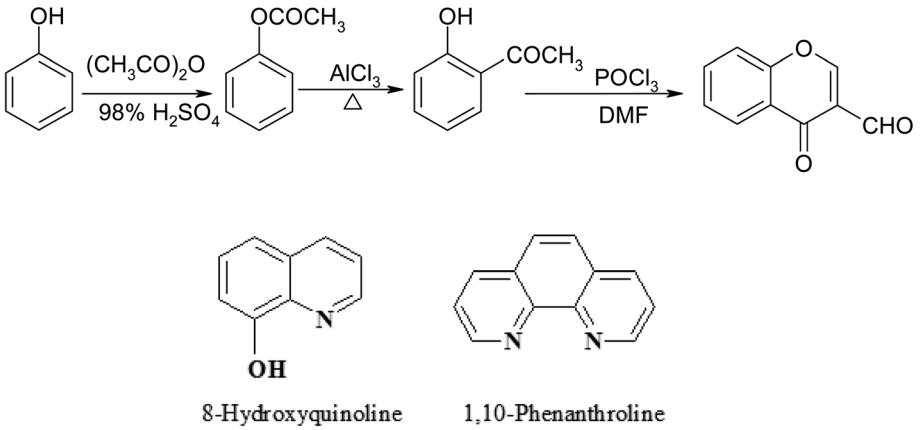

Scheme 1 Synthesis of 3-formylchromone and auxiliary ligands 8-hydroxyquinoline and 1,10-phenanthroline.

Mixed-ligand complexes have lately gained considerable attention due to their important roles in biological processes.[11] The presence of heterocyclic nitrogen donor ligands, such as 1,10-phenanthroline or oxine (8-hydroxyquinoline), has been shown to significantly enhance the various pharmacological impacts of metal complexes.[12]

Nickel and cobalt elements are generally required for life as nickel is involved in a variety of enzymes[13] and cobalt in vitamin B-12 and a number of therapeutics.[14] Their complexes have different biological applications;[15–19] some are used as cisplatin alternatives in cancer treatment[20] and some as catalysts in the oxygenation processes of organic molecules.[21]

In an extension of our continuing interest in the synthesis, spectroscopic characterization and biological activity of chromone-based ligands and their complexes,[22] a series of binary and ternary Ni(II)- and Co(II)-3-formylchromone complexes were synthesized and successfully characterized. Different Ni(II)- and Co(II)-salts (acetate, perchlorate, nitrate, and chloride) were employed to synthesize binary complexes, while auxiliary ligands (Scheme 1), such as N,O-donor oxine or N,N-donor 1,10-phenanthroline, were utilised to synthesize mixed-ligand complexes. Various analytical and spectroscopic techniques were used to characterize the prepared complexes. Theoretical studies were performed on Hyperchem 7.52 software at the *PM3* level and the theoretical findings were compared and correlated with the experimental data. The ligand and its complexes were tested for antibacterial activity.

2. Experimental

2.1. Measurements

IR spectra of the chromone ligand and its complexes were recorded as KBr discs on a FT IR Nicolet IS10 spectrometer. The percentages of C, H and N were estimated on a Vario El-Elementar at the Ministry of Defense, Chemical War Department. A Stuart SMP3 melting point apparatus was utilized to record the decomposition temperatures of the complexes. After decomposing an exact weight of the solid complex with concentrated nitic acid, neutralising with ammonia and titrating with Na_2EDTA, the Ni(II) and Co(II) ions were analysed as described elsewhere.[23] On a GC-2010 Shimadzu gas chromatography mass spectrometer, mass spectra of the metal–chromone complexes were recorded. Electronic spectral measurements were performed as solutions in dimethylformamide and/or Nujol mulls on a Jasco model V-550 UV/Vis spectrophotometer. The Corning conductivity meter NY 14831 model 441 was employed to test the molar conductivity of 10^{-3} M solid complex solutions in dimethylformamide. Magnetic susceptibility measurements for the chromone complexes were done at room temperature with an MKI Johnson Matthey magnetic susceptibility balance (Alpha). The obtained effective magnetic moment values were corrected using Pascal's constants for the diamagnetism of the atoms included in the prepared chelates.[24] On a Shimadzu-50 thermal analyzer, TGA measurements were taken from ambient temperature to 800 °C under N_2 at a heating rate of 10 °C min^{-1}. X-ray diffraction powder patterns of the ligand and its complexes (**2**, **5**, **6**, **7**, **10** and **11**) were recorded at room temperature on a Philips X'Pert powder diffractometer using the Bragg–Brentano configuration and CuKα radiation $\lambda = 1.5406$ Å at the Central Metallurgical Research Institute (CMRDI). The disc diffusion method was used to investigate the biological activities of the chromone ligand and its metal complexes.

2.2. Materials

3-Formylchromone (Scheme 1) was synthesized using a method described in the literature.[25] $Ni(OAc)_2 \cdot 4H_2O$, $Ni(NO_3)_2 \cdot 6H_2O$, $Ni(ClO_4)_2 \cdot 6H_2O$, $NiCl_2 \cdot 6H_2O$, $Co(OAc)_2 \cdot 4H_2O$, $Co(NO_3)_2 \cdot 6H_2O$, $CoCl_2 \cdot 6H_2O$, 8-hydroxyquinoline, oxine (8-HQ), 1,10-phenanthroline, Na_2EDTA, nitric acid, mureoxide, and ammonium hydroxide were purchased from either BDH or Merck. The organic solvents were directly employed without distillation and were reagent grade compounds.

2.3. Synthesis of the metal complexes

The following synthetic procedures are detailed as representative instances and the other complexes were obtained similarly.

2.3.1. $[Ni(L)_2(OAc)_2] \cdot H_2O$, 1. In ~50 mL hot methanol, 0.8 g (4.59 mmol) of ligand L was dissolved. Dropwise, with constant

 © 2022 The Author(s). Published by the Royal Society of Chemistry

Open Access Article. Published on 19 October 2022. Downloaded on 2/8/2026 7:06:59 AM. This article is licensed under a Creative Commons Attribution-NonCommercial 3.0 Unported Licence.

stirring, ~50 mL methanolic solution of 1.143 g (4.59 mmol) $Ni(OAc)_2 \cdot 4H_2O$ was added to this heated ligand solution and the mixture was refluxed for ~10 h, giving a light green precipitate. After cooling to room temperature, the light green solid was filtered, washed with methanol, and dried over anhydrous calcium chloride (yield 50%).

2.3.2. $[Ni(L)(8\text{-}HQ)_2]\cdot 1.5H_2O$, 5. In ~50 mL hot methanol, 0.8 g (4.59 mmol) of the ligand L was dissolved. Dropwise, with constant stirring, ~50 mL methanolic solution of 1.335 g (4.59 mmol) $Ni(NO_3)_2 \cdot 6H_2O$ was added to this heated ligand solution and the mixture was refluxed for ~1 h. Then, 0.667 g (4.59 mmol) of 8-hydroxyquinoline (8-HQ) dissolved in methanol was added to the above mixture and the resultant mixture was heated under reflux for ~10 h, giving a dark green precipitate. After cooling to room temperature, the dark green precipitate was filtered, washed with methanol, and dried over anhydrous calcium chloride (yield 57%).

2.4. Antimicrobial activity

Using the conventional disc-agar diffusion technique,[26,27] the biological activities of the chromone ligand and its complexes were examined. The biological activity was tested against Gram positive bacteria *Staphylococcus aureus* (ATCC 25923) and *Bacillus subtilis* (ATCC 6635), Gram negative bacteria *Salmonella typhimurium* (ATCC 14028) and *Escherichia coli* (ATCC 25922) and fungal strains *Candida albicans* (ATCC 10231) and *Aspergillus fumigatus*. In the case of the Gram-positive and Gram-negative bacteria, the antibiotics chloramphenicol and cephalothin were employed as references, respectively, while in the case of the fungi, cycloheximide was used.

2.4.1. Preparation of tested compounds. The investigated substances were produced in two strengths, 100 and 50 mg mL^{-1}, and dissolved in dimethylformamide (DMF). 10 μL of each preparation of a given concentration was dropped onto a disc with a diameter of 6 mm, resulting in concentrations of 1 and 0.5 mg per disk, respectively. Insoluble compounds were treated after being suspended in DMF and vortexed.

2.4.2. Testing for anti-bacterial and yeast activity. Bacterial cultures were raised at 30 °C in nutrient broth medium. Each bacterium was injected onto the surface of Mueller–Hinton agar plates using a sterile cotton swab after 16 hours of growing at a concentration of 10^8 cells per mL. Then, evenly sized filter paper discs (6 mm in diameter) were carefully placed on the surface of each inoculation plate and impregnated with an equal volume (10 μL) of the specific concentration of dissolved chemicals. The plates were incubated for 24 hours at 36 °C while standing upright. Each extract's activity against each organism was tested three times. Additionally, as negative controls, a suitable solvent was added in place of the dissolved component. Following incubation, the diameters of the growth inhibition zones created around the disc were measured in millimetres using a transparent ruler and averaged and the mean values were tabulated.

2.4.3. Testing for anti-fungal activity. By transferring many loopfuls of spores from the stock cultures into test tubes of sterile distilled water (SDW), which were then stirred and diluted with sterile distilled water to obtain an optical density

Table 1 Analytical and physical data of the Ni(II) and Co(II) complexes of the ligand 3-formylchromone

No.	Reaction	Complex M. F. [F. Wt]	Color	Yield (%)	M. P. (°C)	Elemental analysis, % found/(calc.) C	H	N/S	M
1	L + $Ni(OAc)_2 \cdot 4H_2O$	$[Ni(L)_2(OAc)_2]\cdot H_2O$ $C_{24}H_{20}O_{11}Ni$ [543.13]	Light green	50	>300	52.86 (53.08)	4.52 (3.71)	—	10.70 (10.81)
2	L + $Ni(NO_3)_2 \cdot 6H_2O$	$[Ni(L)_3](NO_3)_2 \cdot 0.5MeOH$ $C_{30.5}H_{20}N_2O_{15.5}Ni$ [721.21]	Light green	48	253–257	52.82 (50.80)	3.30 (2.80)	4.10 (3.88)	7.92 (8.14)
3	L + $Ni(ClO_4)_2 \cdot 6H_2O$	$[Ni(L)_2(H_2O)_2](ClO_4)_2\cdot H_2O$ $C_{20}H_{18}O_{17}Cl_2Ni$ [659.97]	Green	45	[a]	36.41 (36.40)	2.30 (2.75)	—	[a] (8.90)
4	L + $NiCl_2.6H_2O$	$[Ni(L)_2Cl_2(H_2O)_2]$ $C_{20}H_{12}O_6Cl_2Ni$ [477.93]	Pale lemon	83	>300	50.01 (50.26)	2.90 (2.53)	—	12.10 (12.28)
5	L + $Ni(NO_3)_2 \cdot 6H_2O$ + 8-HQ	$[Ni(L)(8\text{-}HQ)_2]\cdot 1.5H_2O$ $C_{28}H_{21}N_2O_{6.5}Ni$ [548.20]	Dark green	57	>300	60.80 (61.35)	3.73 (3.86)	5.60 (5.11)	10.40 (10.71)
6	L + $Ni(NO_3)_2 \cdot 6H_2O$ + Phen	$[Ni(L)(Phen)(H_2O)(MeOH)](NO_3)_2$ $C_{23}H_{19}N_3O_{12}Ni$ [588.13]	Pale green	45	156	47.30 (46.97)	3.87 (3.26)	7.60 (7.14)	9.61 (9.98)
7	L + $Co(OAc)_2 \cdot 4H_2O$	$[Co(L)_2(OAc)_2]\cdot 1.5H_2O$ $C_{24}H_{21}O_{11.5}Co$ [552.36]	Light orange	47	>300	52.44 (52.19)	4.14 (3.83)	—	10.30 (10.67)
8	L + $Co(NO_3)_2 \cdot 6H_2O$	$[Co(L)_3](NO_3)_2\cdot MeOH$ $C_{31}H_{22}N_2O_{16}Co$ [737.46]	Orange	61	>300	50.90 (50.49)	3.40 (3.01)	3.40 (3.80)	7.70 (7.99)
9	L + $CoCl_2 \cdot 6H_2O$	$[Co(L)_2Cl_2]$ $C_{20}H_{12}O_6Cl_2Co$ [478.15]	Orange	40	>300	50.70 (50.24)	3.00 (2.53)	—	12.10 (12.33)
10	L + $Co(NO_3)_2 \cdot 6H_2O$ + 8-HQ	$[Co(L)(8\text{-}HQ)_2]\cdot 1.5H_2O$ $C_{28}H_{21}N_2O_{6.5}Co$ [548.42]	Dark brown	87	>300	60.90 (61.32)	3.75 (3.86)	5.70 (5.11)	10.50 (10.75)
11	L + $Co(NO_3)_2 \cdot 6H_2O$ + Phen	$[Co(L)(Phen)(MeOH)_2](NO_3)_2$ $C_{24}H_{21}N_3O_{12}Co$ [602.38]	Rose	50	130	48.10 (47.85)	3.77 (3.51)	7.31 (6.98)	9.65 (9.78)

[a] Not determined.

Open Access Article. Published on 19 October 2022. Downloaded on 2/8/2026 7:06:59 AM.
This article is licensed under a Creative Commons Attribution-NonCommercial 3.0 Unported Licence.

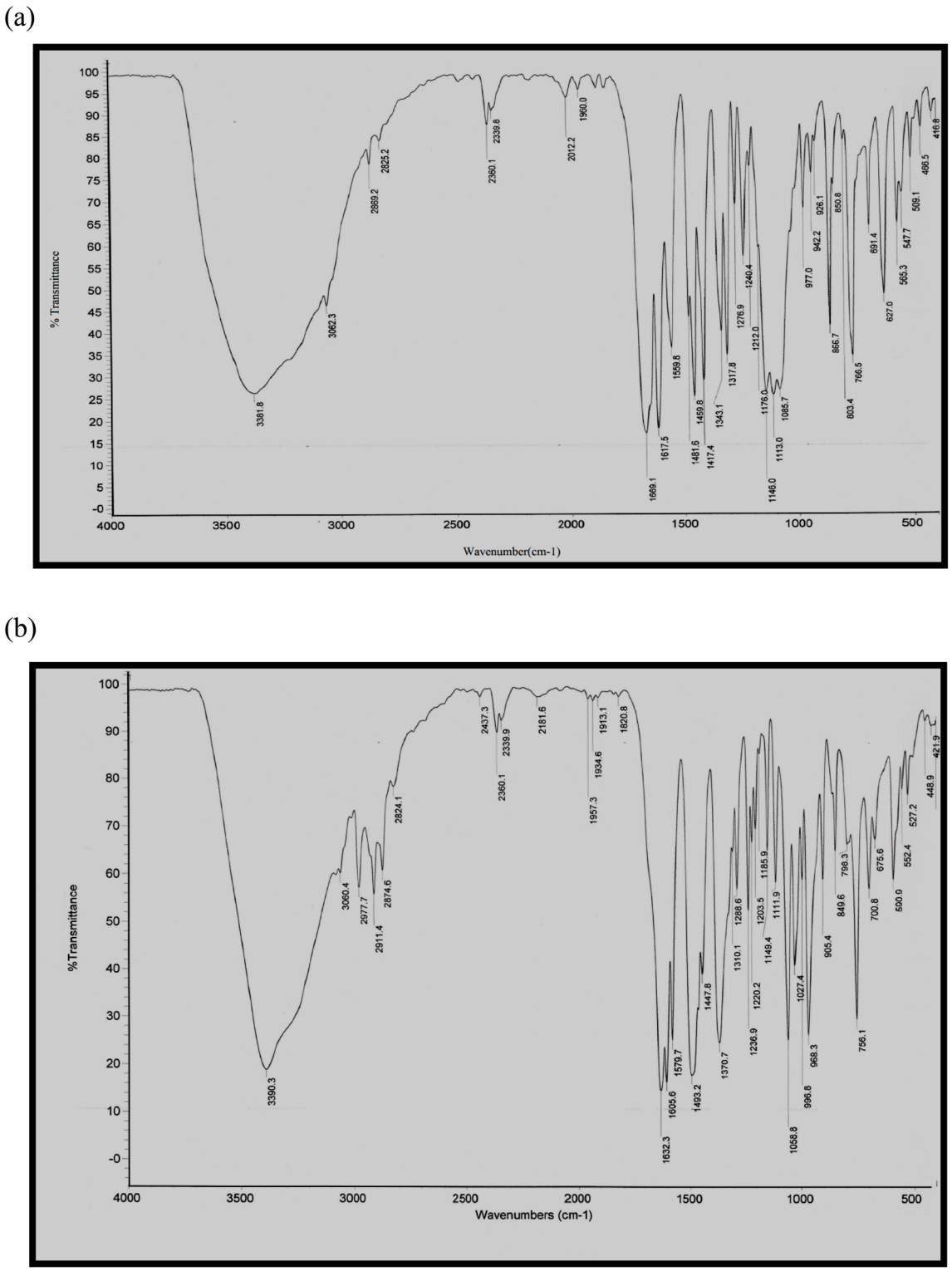

Fig. 1 (a) IR spectrum of $[Ni(L)_2(H_2O)_2](ClO_4)_2 \cdot H_2O$ (**3**). (b) IR spectrum of $[Ni(L)_2Cl_2(H_2O)_2]$ (**4**).

corresponding to 2.0×10^5 spore per mL, an active sample for tests was created. A consistently spaced sample of 0.1 percent suspension was swabbed and dried for 5 minutes, then the identical steps as previously were performed.

2.4.4. Standard references. For the Gram-positive bacteria, Gram-negative bacteria, and yeast and fungi, respectively, the antibiotics cycloheximide, cephalothin, and chloramphenicol were utilised as standard references.

© 2022 The Author(s). Published by the Royal Society of Chemistry

Open Access Article. Published on 19 October 2022. Downloaded on 2/8/2026 7:06:59 AM.
This article is licensed under a Creative Commons Attribution-NonCommercial 3.0 Unported Licence.

2.5. Molecular docking and modeling

Molecular docking studies for the compounds were tested against *S. aureus* nucleoside diphosphate kinase, PDB ID: 3Q89, using the MOE 2014.0901 software.

Geometrical optimization and conformation analysis were performed using the *PM3* forcefield as implemented in Hyperchem 7.52 (ref. 28) in order to acquire a better understanding of the molecular structure of the chromone ligand and its complexes.

3. Results and discussion

To investigate the influence of counter ions on the products, the chromone ligand was reacted with numerous salts of nickel(II) and cobalt(II) ions (acetate, perchlorate, nitrate, and chloride). Reactions of nickel(II) and cobalt(II) nitrates with the chromone ligand in the presence of auxiliary ligands (8-hydroxyquinoline or 1,10-phenanthroline) gave mixed-ligand complexes. The obtained complexes have good storage qualities, *i.e.* they are non-hygroscopic and sparingly soluble in water and most common organic solvents except dimethylformamide. Table 1 summarizes the main analytical and physical data of the chromone ligand along with its nickel(II) and cobalt(II) complexes.

3.1. IR spectra

The IR spectra of some representative metal complexes are depicted in Fig. 1a and b and the characteristic IR spectral bands are tabulated in Table 2. The IR spectra of the complexes are compared to that of the ligand to identify the coordinating sites and their extent. This comparison revealed the following: (i) the spectra of the complexes exhibited strong and broad bands in the range 3296-3535 cm^{-1} which can be ascribed to the ν(OH) of the coordinated or non-coordinated water and/or methanol molecules in the complexes. (ii) The strong bands located at 1694 and 1643 cm^{-1} assigned to ν(HC = O) and ν(C=O), respectively, of the chromone ligand exhibited red shifts in

Table 2 Characteristic IR spectral data of the ligand and its Ni(II) and Co(II) complexes

		IR spectra (cm^{-1})					
No.	Complex	ν(OH)	ν(HC=O)	ν(C=O)	ν(M–O)	ν(M–N)	Other bands
	L	—	1694	1643	—	—	—
1	$[Ni(L)_2(OAc)_2]\cdot H_2O$	3535	1629	1606	528	—	1493 $\nu_{as}(COO^-)$, 1318 $\nu_s(COO^-)$; (monodentate OAc^-)
2	$[Ni(L)_3](NO_3)_2\cdot 0.5MeOH$	3296	1628	1607	528	—	1447; $\nu(NO_3^-)$ (ionic)
3	$[Ni(L)_2(H_2O)_2](ClO_4)_2\cdot H_2O$	3382	1669	1618	509	—	1086, 627; $\nu(ClO_4^-)$ (ionic)
4	$[Ni(L)_2Cl_2(H_2O)_2]$	3390	1632	1606	527	—	
5	$[Ni(L)(8\text{-}HQ)_2]\cdot 1.5H_2O$	3385	1629	1581	501	450	1504; ν(C=N) 8-HQ
6	$[Ni(L)(Phen)(H_2O)(MeOH)](NO_3)_2$	3357	1673	1619	567	428	1427; $\nu(NO_3^-)$ (ionic), 1518; ν(C=N) Phen
7	$[Co(L)_2(OAc)_2]\cdot 1.5H_2O$	3523	1625	1606	528	—	1490 $\nu_{as}(COO^-)$, 1319 $\nu_s(COO^-)$; (monodentate OAc^-)
8	$[Co(L)_3](NO_3)_2\cdot MeOH$	3523	1626	1605	528	—	1446; $\nu(NO_3^-)$ (ionic)
9	$[Co(L)_2Cl_2]$	3521	1628	1605	528	—	
10	$[Co(L)(8\text{-}HQ)_2]\cdot 1.5H_2O$	3385	1633	1604	539	424	1501; ν(C=N) 8-HQ
11	$[Co(L)(Phen)(MeOH)_2](NO_3)_2$	3309	1646	1613	505	427	1425; $\nu(NO_3^-)$ (ionic), 1517; ν(C=N) Phen

Table 3 Electronic spectra, magnetic moments and molar conductivity data of the ligand and its Ni(II) and Co(II) complexes

No.	Complex	Electronic spectral bands[a] (nm), λ_{max}[a] (nm)/(ε_{max}, L cm^{-1} mol^{-1})	μ_{eff} (B.M.)	Conductance[a] (Ω^{-1} cm^2 mol^{-1})
	L	271 (4340), 353 (4700), 387 (3415)	—	—
1	$[Ni(L)_2(OAc)_2]\cdot H_2O$	(500 sh)[b]	2.80	10.6
2	$[Ni(L)_3](NO_3)_2\cdot 0.5MeOH$	(500 sh, 613 sh)[b]	3.20	106.3
3	$[Ni(L)_2(H_2O)_2](ClO_4)_2\cdot H_2O$	(470 sh, 504, 605sh)[b]	2.83	125.0
4	$[Ni(L)_2Cl_2(H_2O)_2]$	(400, 502, 630)[b]	2.43	18.5
5	$[Ni(L)(8\text{-}HQ)_2]\cdot 1.5H_2O$	(493, 693)[b]	2.00	44.2
6	$[Ni(L)(Phen)(H_2O)(MeOH)](NO_3)_2$	(504, 605)[b]	2.30	122.8
7	$[Co(L)_2(OAc)_2]\cdot 1.5H_2O$	(505 sh)[b]	4.74	9.5
8	$[Co(L)_3](NO_3)_2\cdot MeOH$	(510)[b]	5.21	103.2
9	$[Co(L)_2Cl_2]$	(532 sh)[b]	4.34	6.40
10	$[Co(L)(8\text{-}HQ)_2]\cdot 1.5H_2O$	(488)[b]	2.00	44.8
11	$[Co(L)(Phen)(MeOH)_2](NO_3)_2$	(500 sh)[b]	3.86	108.1

[a] Solutions in DMF (10^{-3} M). [b] Nujol mull.

Open Access Article. Published on 19 October 2022. Downloaded on 2/8/2026 7:06:59 AM.
This article is licensed under a Creative Commons Attribution-NonCommercial 3.0 Unported Licence.

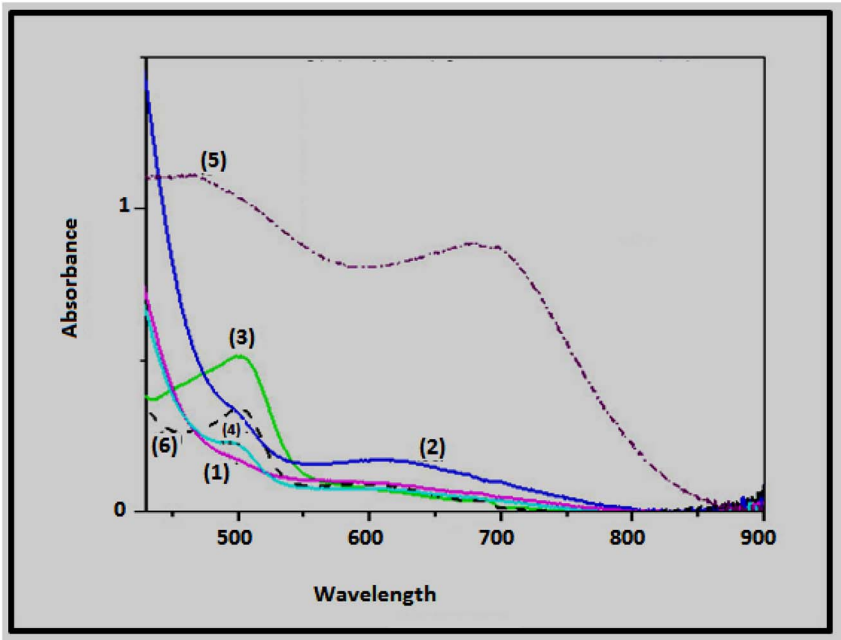

Fig. 2 Electronic spectra of some representative nickel(II) complexes (**1–6**) as Nujol mulls.

the complexes, revealing the involvement of these groups in complexation.[29] The extent of carbonyl coordination could be seen by the negative slope of the linear correlation of ΔE_{gab}, which is analogous with the stability of the complex (*vide infra*), *versus* the stretching frequency of carbonyl. For complexes **1**, **3**, **5**, **8**, and **11**, ΔE_{gab} (eV) = 65.2–0.0367 ν(C=O)/cm^{-1}, r = 0.96; *i.e.*, as the extent of carbonyl coordination with the metal ion increases, the carbonyl bond is elongated and the frequency shifts lower, as shown by the negative slope. (iii) Participation of the anions and their modes of bonding was investigated using the infra-red spectral data. The acetato-complexes (**1** and **7**) displayed new bands at 1493 and 1490 (**1**) and 1318 and 1319 cm^{-1} (**7**), which may be respectively attributed to the ν_{as}(COO$^-$) and ν_s(COO$^-$) of the acetate group.[30] The separation between the two bands, $\Delta\nu = (\nu_{as} - \nu_s)$, demonstrates the monodentate nature of the acetate group.[31] In complexes **2**, **6**, **8** and **11**, the new bands observed in the range 1425–1447 cm^{-1} may be those of the ionic nitrate group.[32] In complex **3**, the new bands observed at 1086 and 627 cm^{-1} may be related to the ν_3 and ν_4 vibrations, respectively, of the ionic perchlorate group.[33] The direct coordination of the acetate anion as well as the ionic nature of the nitrate and perchlorate anions is supported by molar conductivity data (see Section 3.2). (iv) The spectra of ternary complexes (**5**, **6**, **10** and **11**) displayed new bands in the range 1501–1518 cm^{-1} which may be ascribed to the coordination of the C=N group of the 8-HQ or 1,10-Phen ligands to the nickel or cobalt.[34] (v) The new bands observed in the ranges 501–567 and 424–450 cm^{-1} may be attributed to ν(Ni- or Co–O) and ν(Ni- or Co–N), respectively.[35,36]

3.2. Conductivity measurements

Based on the molar conductance values of the complexes in dimethylformamide (Table 3), the complexes can be divided into two classes: (i) non-electrolytes (complexes **1**, **4**, **5**, **7**, **9** and **10**) with molar conductance values in the range 6.40–44.8 Ω^{-1} cm^2 mol^{-1} and (ii) 2 : 1 electrolytes (complexes **2**, **3**, **6**, **8** and **11**) with molar conductance values in the range 103.2–125 Ω^{-1} cm^2 mol^{-1}.[37] This finding agrees with the weak coordinating capability of the nitrate and perchlorate anions as compared to the strong coordinating capability of the acetate anion. Furthermore, this finding is in agreement with the infrared spectral data (see Section 3.1), illustrating the coordinated nature of the acetate group and the ionic nature of the nitrate and perchlorate groups.

3.3. Magnetic moment measurements and electronic spectra

The electronic spectral data and magnetic moment values of the chromone ligand and its nickel(II) and cobalt(II) complexes are tabulated in Table 3; Fig. 2 presents the electronic spectra of some representative complexes. The chromone nickel(II) complexes (with the exception of **4–6**) have magnetic moment values in the range of 2.80–3.20 B.M., demonstrating an octahedral geometry.[38] However, the magnetic moment values of complexes **4–6** are in the range of 2.00–2.43 B.M., indicating an octahedral geometry with an antiferromagnetic interaction or an equilibrium between square and octahedral species.[39] This explanation is further supported by the electronic spectra of the nickel(II) complexes showing two bands in the ranges of 493–504 and 605–693 nm which may be respectively assigned to the $^3A_{2g}(F) \rightarrow {}^3T_{1g}(P)$ and $^3A_{2g}(F) \rightarrow {}^3T_{1g}(F)$ electronic transitions in octahedral geometrical arrangements of Ni(II) ion.[40]

The magnetic moment values of the chromone cobalt(II) complexes (except **9–11**) are in the range 4.74–5.21 B.M., consistent with octahedral cobalt(II) complexes (4.8–5.2 B.M.).[38] The lower values (Table 3) of complexes **9–11** could be attributed to antiferromagnetic interaction.[41] The electronic spectra

© 2022 The Author(s). Published by the Royal Society of Chemistry

Open Access Article. Published on 19 October 2022. Downloaded on 2/8/2026 7:06:59 AM.
This article is licensed under a Creative Commons Attribution-NonCommercial 3.0 Unported Licence.

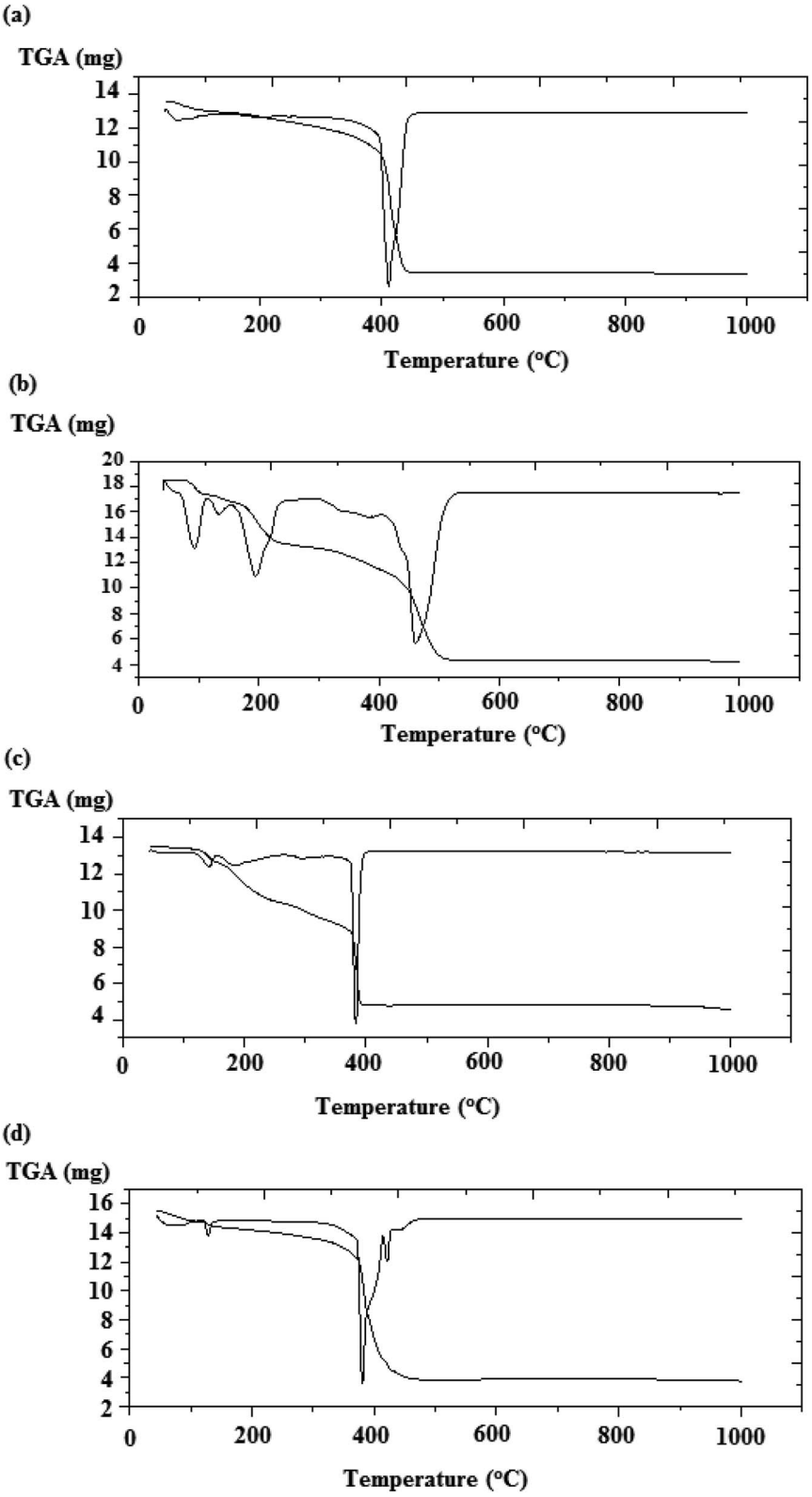

Fig. 3 (a) TGA–DrTGA curves of $[Ni(L)(8\text{-}HQ)_2]\cdot 1.5H_2O$ (**5**). (b) TGA–DrTGA curves of $[Ni(L)(Phen)(H_2O)(MeOH](NO_3)_2$ (**6**). (c). TGA–DrTGA curves of $[Co(L)_2(OAc)_2]\cdot H_2O$ (**7**). (d) TGA–DrTGA curves of $[Co(L)(8\text{-}HQ)]NO_3\cdot 1.5H_2O$ (**10**).

Open Access Article. Published on 19 October 2022. Downloaded on 2/8/2026 7:06:59 AM. This article is licensed under a Creative Commons Attribution-NonCommercial 3.0 Unported Licence.

Table 4 Thermal analysis data of selected metal complexes

Complex	Temperature range (°C)	% Wt loss Found/(calc.)	Lost fragment (no. of molecules)
$[Ni(L)_3](NO_3)_2\cdot 0.5MeOH$ (**2**)	43–132	1.67/(2.22)	0.5MeOH (solv.)
$[Ni(L)(8\text{-}HQ)_2]\cdot 1.5H_2O$ (**5**)	45–142	4.27/(4.93)	$1.5H_2O$ (hyd.)
$[Ni(L)(Phen)(H_2O)(MeOH)](NO_3)_2$ (**6**)	42–116	5.93/(5.44)	1MeOH (coord.)
	116–156	2.97/(3.06)	$1H_2O$ (coord.)
	156–336	21.1/(21.40)	$2HNO_3$
$[Co(L)_2(OAc)_2]\cdot 1.5H_2O$ (**7**)	45–138	5.10/(4.89)	$1.5H_2O$ (hyd.)
	138–309	21.6/(21.72)	2AcOH
$[Co(L)(8\text{-}HQ)_2]\cdot 1.5H_2O$ (**10**)	44–117	4.34/(4.92)	$1.5H_2O$ (hyd.)

Table 5 Temperatures of decomposition and the kinetic parameters of selected complexes

Complex	Step	n order	T (K)	A (S^{-1})	ΔE (kJ mol^{-1})	ΔH (kJ mol^{-1})	ΔS (kJ mol^{-1} K^{-1})	ΔG (kJ mol^{-1})
$[Ni(L)_3](NO_3)_2\cdot 0.5MeOH$ (**2**)	First	1	349	2.13×10^6	1.0267	−1.87	−0.190	64.68
$[Ni(L)(8\text{-}HQ)_2]\cdot 1.5H_2O$ (**5**)	First	1	356	9.75×10^3	29.160	26.20	−0.290	130.50
$[Ni(L)(Phen)(H_2O)(MeOH)](NO_3)_2$ (**6**)	First	1	367	2.76×10^{13}	106.09	103.0	2.37×10^{-3}	102.16
	Second	1	404	1.14×10^6	64.650	61.25	−0.139	117.37
$[Co(L)_2(OAc)_2]\cdot 1.5H_2O$ (**7**)	First	1	363	1.9×10^3	1.0816	−1.94	−0.192	67.76
$[Co(L)(8\text{-}HQ)_2]\cdot 1.5H_2O$ (**10**)	First	0	353	2.57×10^9	84.160	81.20	−0.074	107.37

of cobalt(II) complexes revealed a band in the 488–532 nm range which might be attributed to the $^4T_{1g} \rightarrow {}^4T_{1g}(P)$ transition in an octahedral geometry.[31,39] The negative slope of ΔE_{gab} with λ_{max}, as ΔE_{gab} is known to increase with the increasing stability of complexes, leads to a decreasing in λ_{max}, where $\Delta E_{gab} = 8.35$ (0.4251)–0.00443 (0.0007426) λ_{max}, $r = 92.2\%$, for complexes **1–4** and **11**.

3.4. Thermal analysis

The TGA analysis of the chromone complexes, using **2**, **5–7** and **10** as examples, were measured from room temperature to 800 °C with a heating rate of 10 °C min^{-1}. Fig. 3a–d represent the thermal analysis data of **5–7** and **10** and the thermal data are summarized in Table 4.

The initial degradation step of the chromone complexes observed in the range 42–142 °C corresponds to the elimination of solvated molecules. The second degradation step in the range 116–309 °C agrees with the elimination of coordinated water or acetic acid molecules. In the case of complex **6**, the third degradation step in the range 156–336 °C corresponds to the elimination of two nitric acid molecules. The decomposition processes of complex **6** are summarized in Scheme 4.

Furthermore, using the Coats–Redfern equations,[42] the order n and activation parameters of the major degradation processes of the metal–chromone complexes were derived from the TG thermograms and the kinetic parameters are tabulated in Table 5. Based on the data in Table 5, it is possible to conclude the following points: (i) the decomposition processes are endothermic, as evidenced from the +ve ΔH values. (ii) The autocatalytic effect of nickel or cobalt ions on the thermal degradation of the complexes and the non–spontaneous processes is indicated by ΔG values that are comparatively low and have a +ve sign.[43] (iii) ΔS values for complexes are -ve, demonstrating that the activated complex is more ordered than the reactants and/or the reactions are slow.[44] (iv) In the ternary cobalt–phen complex (**6**), the value of activation energy E for the second stage of degradation is smaller than that of the first stage, demonstrating that the rate of decomposition of the second stage is higher than that of the first.[45]

3.5. Mass spectra

As illustrative examples, the mass spectra of complexes **4**, **6**, **7** and **10** were recorded to assign the most abundant molecular ion peaks. The mass spectra of complexes **4** and **6** are shown in Fig. 4a and b, respectively. For complexes **4** and **6**, the observed highest mass peaks at m/z 478 and 589, respectively, are in good agreement with the formula weights of the complexes $[Ni(L)_2Cl_2(H_2O)_2]$ (F. Wt = 477.93) and $[Ni(L)(Phen)(H_2O)(MeOH)](NO_3)_2$ (F. Wt = 588.13). For the mass spectra of complexes **7** and **10**, the observed molecular ion peaks at m/z 525 and 521, respectively, are consistent with the formula weights of the anhydrous complexes $[Co(L)_2(OAc)_2]$ (F. Wt = 525.36) and $[Co(L)(8\text{-}HQ)_2]$ (F. Wt = 521.42).

Based on the above interpretation, structures of the binary and ternary metal–chromone complexes are represented in Schemes 2 and 3.

3.6. Powder XRD measurements

Powder XRD measurements of the ligand and complexes **2**, **5**, **6**, **7**, **10** and **11** (Fig. 5) showed several peaks with different

 © 2022 The Author(s). Published by the Royal Society of Chemistry

Open Access Article. Published on 19 October 2022. Downloaded on 2/8/2026 7:06:59 AM.
This article is licensed under a Creative Commons Attribution-NonCommercial 3.0 Unported Licence.

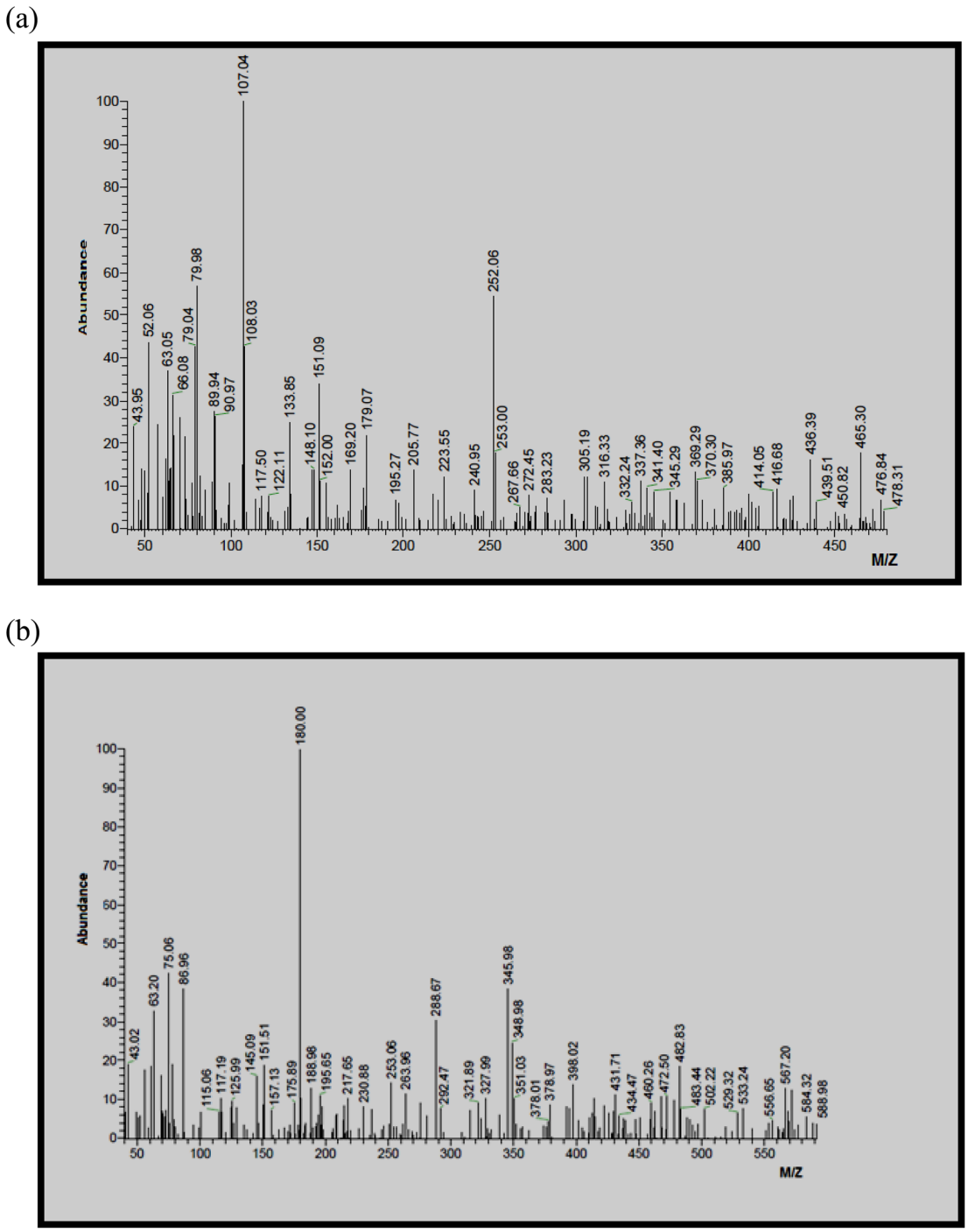

Fig. 4 (a) Mass spectrum of the complex $[Ni(L)_2Cl_2(H_2O)_2]$ (**4**). (b) Mass spectrum of the complex $[Ni(L)(Phen)(H_2O)(MeOH)](NO_3)_2$ (**6**).

intensities in the 2θ range from 0 to 80°, representing that the materials are crystalline, except for complex **2** which has an amorphous structure. The diffractograms and associated data depict the 2θ value for each peak, the relative intensity of the Co(II)- and Ni(II)-complexes to that of the ligand. This result suggests that the Co(II) and Ni(II) ions were coordinated to the ligand L to give new complexes. The main crystallite sizes of the most intense peak are 11.18, 27.59, 16.90, 102.09 and 11.11 nm for ligand complexes **5**, **6**, **7**, **10** and **11**, respectively.

3.7. Antimicrobial activity

The antimicrobial effects of the obtained Ni(II)- and Co(II)-chromone complexes were assessed against Gram +ve bacteria *Staphylococcus aureus* and *Bacillus subtilis*, Gram −ve bacteria *Escherichia coli* and *Salmonella typhimurium*, the yeast *Candida albicans* and the fungus *Aspergillus fumigatus* (Table 6). From the data in Table 6, the following points are deduced: (i) all complexes are biologically active except complexes **5** and **10**,

Open Access Article. Published on 19 October 2022. Downloaded on 2/8/2026 7:06:59 AM.
This article is licensed under a Creative Commons Attribution-NonCommercial 3.0 Unported Licence.

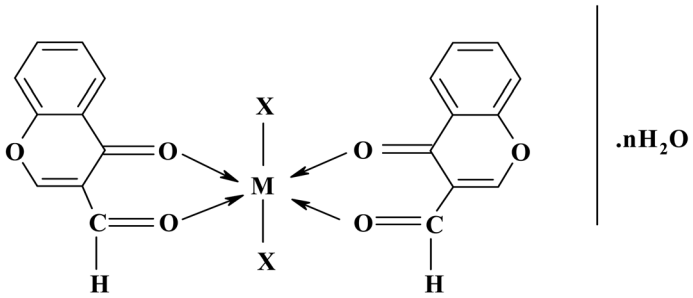

X	n	M	Complex
OAc	1	Ni	**1**
Cl	nil	Ni	**4**
OAc	1.5	Co	**7**
Cl	nil	Co	**9**

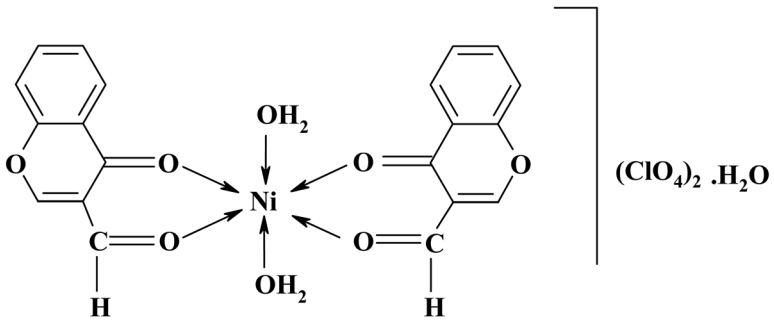

(3)

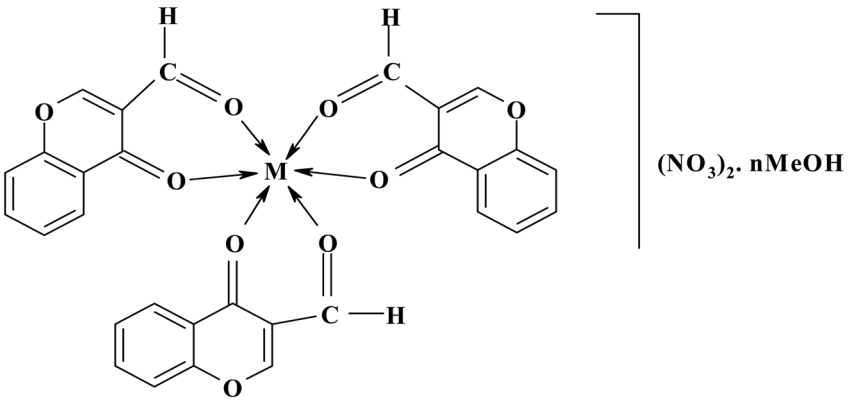

n	M	Complex
0.5	Ni	**2**
1	Co	**8**

Scheme 2 Proposed structures of binary Ni(II) and Co(II) complexes.

which are inactive towards all organisms. (ii) Some complexes are inactive towards certain organisms, as follows: towards *Staphylococcus aureus*, complexes **3** and **9** are inactive, and towards *Salmonella typhimurium*, complex **6** is inactive. (iii) The bioactivity of the present complexes ranges from poor to a high nearly equivalent to that of the control. (iv) Against *Staphylococcus aureus*, all complexes exhibited poor activity except the ternary Co(II)–Phen complex **11**, which showed high activity. On

© 2022 The Author(s). Published by the Royal Society of Chemistry

Open Access Article. Published on 19 October 2022. Downloaded on 2/8/2026 7:06:59 AM.
This article is licensed under a Creative Commons Attribution-NonCommercial 3.0 Unported Licence.

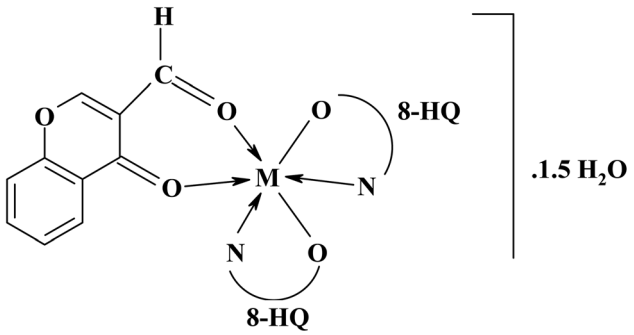

M	Complex
Ni	**5**
Co	**10**

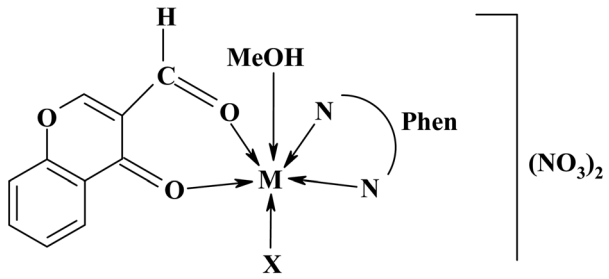

X	M	Complex
H_2O	Ni	**6**
MeOH	Co	**11**

Scheme 3 Proposed structures of ternary Ni(II) and Co(II) complexes.

the other hand, most complexes exhibited high activity towards *Bacillus subtilis* and the highest activity was observed in the acetato- (**1**) and chloro- (**4**) nickel(II) complexes. (v) Against *Salmonella typhimurium*, most complexes exhibited poor to intermediate activity and the highest activity was given by the acetato-Ni(II) complex **1**. The complexes exhibited intermediate to high activity towards *Escherichia coli* and the highest activity is given by the perchlorate-Ni(II) complex **3**. (vi) Against *Candida albicans* and *Aspergillus fumigates*, the complexes exhibited intermediate to high activity and the highest activities are given by the acetato-Ni(II) complex **1** (in the case of *Candida albicans*) and the chloro-Co(II) complex **9** and the ternary Co(II)–Phen complex **11** (in the case of *Aspergillus fumigates*).

It has been reported that different parameters, including the characters of the chelating agent and its chelating donor atoms, the character of the metal ion, the geometrical arrangement of the complex, solubility, and other characteristics, have a major impact on the antibacterial activity exhibited by a compound.[46]

3.8. Molecular docking studies

The MOE 2014.0901 software was used for molecular docking studies for the ligand L and its complexes **2**, **6**, **8** and **11**. Elena *et al.* studied molecular docking for chromone compounds using the *S. aureus* nucleoside diphosphate kinase (PDB ID: 3Q89) (Table 7).[47]

The ligand (Fig. 6a) formed three bonds with amino acid residues; one of them is the H-acceptor bond between O7 of L and LYS 9 (2.98 Å, −0.8 kcal mol^{-1}). The second and third bonds are coordinate bonds between O11 and O14 of L and MG 159 (2.37 Å, −1.9 kcal mol^{-1} and 4.51 Å, −2.4 kcal mol^{-1}, respectively).

On the other hand, Ni(II)-complex **2** (Fig. 6b) formed three bonds. The first and second are H-acceptor bonds between O28 and O43 and LYS 9 and ASN 112 (2.95 Å, −18.0 kcal mol^{-1} and 3.19 Å, −2.1 kcal mol^{-1}, respectively). The third bond is a pi-cation between the 6-ring and ARG 102 (3.56 Å, −0.8 kcal mol^{-1}). Ni(II)-complex **6** (Fig. 6c) formed two bonds with the amino acid residues, the first being an H-acceptor bond between O30 and HIS 52 (2.89 Å, −14.0 kcal mol^{-1}) and the second an ionic bond between Ni and MG 159 (1.52 Å, −28.5 kcal mol^{-1}).

Co(II)-complex **8** (Fig. 6d) formed two bonds with the amino acid residues, H-acceptor bonds between O28 and O43 and LYS 9 and ASN 112 (2.97 Å, −18.6 kcal mol^{-1} and 3.12 Å, −2.8 kcal mol^{-1}, respectively). Co(II)-complex **11** (Fig. 5e) formed two bonds with the amino acid residues in the active site of the protein. The first is an H-acceptor between O30 and HIS 52 (3.40 Å, −1.7 kcal mol^{-1}). The second is an ionic bond between CO29 and MG 159 (1.47 Å, −30.3 kcal mol^{-1}).

According to Hansch and Leo, highly lipophilic compounds will participate in the lipid interior of membranes and be retained there. A drug has low solubility with a higher log *P* and has difficulty penetrating lipid membranes with a lower log *P*.[48] Lipophilicity (log *P*) is a feature that affects absorption, solubility, distribution, excretion qualities, metabolism, and pharmacological activity; normalized B.S. and normalized C.A. rise as log *P* increases.

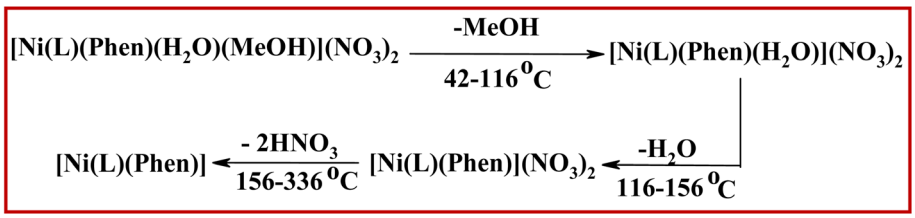

Scheme 4 Thermal degradation pattern of complex **6**, $[Ni(L)(Phen)(H_2O)(MeOH](NO_3)_2$ in the range 42–336 °C.

Open Access Article. Published on 19 October 2022. Downloaded on 2/8/2026 7:06:59 AM.
This article is licensed under a Creative Commons Attribution-NonCommercial 3.0 Unported Licence.

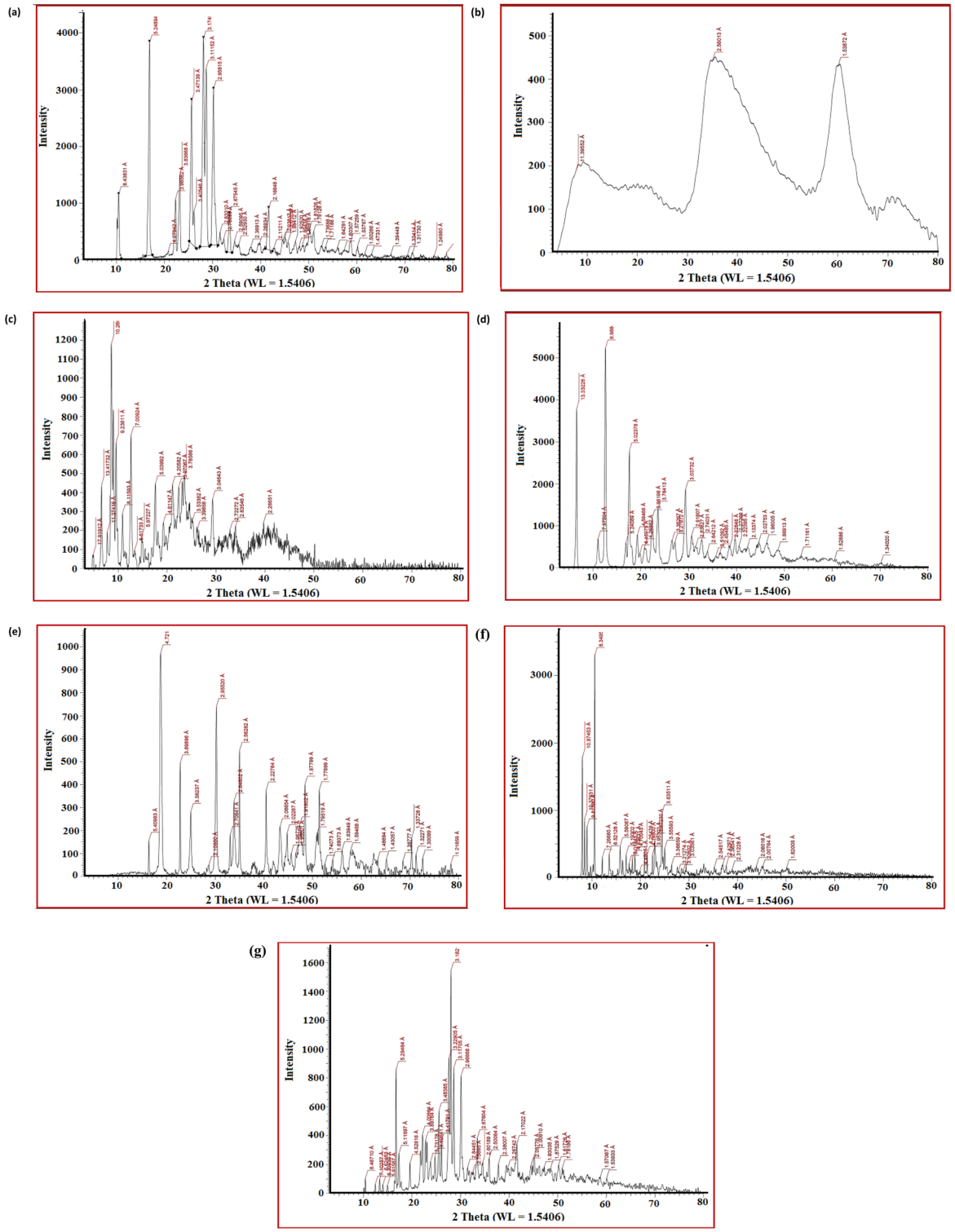

Fig. 5 (a) X-ray diffraction (XRD) pattern of the ligand. (b) X-ray diffraction (XRD) pattern of $[Ni(L)_3](NO_3)_2 \cdot 0.5MeOH$ (**2**). (c) X-ray diffraction (XRD) pattern of $[Ni(L)(8\text{-}HQ)_2] \cdot 1.5H_2O$ (**5**). (d) X-ray diffraction (XRD) pattern of $[Ni(L)(Phen)(H_2O)(MeOH)](NO_3)_2$ (**6**). (e) X-ray diffraction (XRD) pattern of $[Co(L)_2(OAc)_2] \cdot 1.5H_2O$ (**7**). (f) X-ray diffraction (XRD) pattern of $[Co(L)(8\text{-}HQ)_2] \cdot 1.5H_2O$ (**10**). (g) X-ray diffraction (XRD) pattern of $[Co(L)(Phen)(MeOH)_2](NO_3)_2$ (**11**).

© 2022 The Author(s). Published by the Royal Society of Chemistry

Open Access Article. Published on 19 October 2022. Downloaded on 2/8/2026 7:06:59 AM.
This article is licensed under a Creative Commons Attribution-NonCommercial 3.0 Unported Licence.

Table 6 Antimicrobial activity of the ligand and its metal complexes against Gram-positive bacteria, Gram-negative bacteria, yeast and fungi using disc diffusion method[a]

Organism		Mean[b] of zone diameter, nearest whole mm											
		Gram-positive bacteria				Gram-negative bacteria				Yeast and fungi[c]			
		Staphylococcus aureus (ATCC 25923)		*Bacillus subtilis* (ATCC 6635)		*Salmonella typhimurium* (ATCC 14028)		*Escherichia coli* (ATCC 25922)		*Candida albicans* (ATCC 10231)		*Aspergillus fumigatus*	
Sample	Concentration	1 mg ml^{-1}	0.5 mg ml^{-1}	1 mg ml^{-1}	0.5 mg ml^{-1}	1 mg ml^{-1}	0.5 mg ml^{-1}	1 mg ml^{-1}	0.5 mg ml^{-1}	1 mg ml^{-1}	0.5 mg ml^{-1}	1 mg ml^{-1}	0.5 mg ml^{-1}
L		22 I	19H	31H	27H	29H	26H	24 I	20H	43H	38H	25 I	20H
$[Ni(L)_2(OAc)_2]\cdot H_2O$ (**1**)		9 L	8L	26H	23H	15I	12I	17I	15I	26H	23H	25H	22H
$[Ni(L)_3](NO_3)_2\cdot 0.5MeOH$ (**2**)		10L	9L	25H	21H	11L	9L	15I	12I	24H	20H	26H	22H
$[Ni(L)_2(H_2O)_2](ClO_4)_2\cdot H_2O$ (**3**)		—	—	25H	22H	11L	8L	21I	18H	24H	19H	22I	18I
$[Ni(L)_2Cl_2(H_2O)_2]$ (**4**)		9L	7L	26H	23H	9L	7L	16I	11I	25H	19H	20I	16I
$[Ni(L)(8\text{-}HQ)_2]\cdot 1.5H_2O$ (**5**)		—	—	—	—	—	—	—	—	—	—	—	—
$[Ni(L)(Phen)(H_2O)(MeOH)](NO_3)_2$ (**6**)		11L	8L	26H	22H	—	—	11L	9L	24H	19H	18I	16I
$[Co(L)_2(OAc)_2]\cdot 1.5H_2O$ (**7**)		9 L	8L	20I	18H	11L	9L	12I	10I	24H	22H	16I	14I
$[Co(L)_3](NO_3)_2\cdot MeOH$ (**8**)		11L	8L	21I	18H	10L	8L	13I	10I	24H	20H	18I	14I
$[Co(L)_2Cl_2]$ (**9**)		—	—	22I	18H	8L	7L	14I	10I	20I	16I	27H	23H
$[Co(L)(8\text{-}HQ)_2]\cdot 1.5H_2O$ (**10**)		—	—	—	—	—	—	—	—	—	—	—	—
$[Co(L)(Phen)(MeOH)_2](NO_3)_2$ (**11**)		23I	20H	23I	18H	11L	9L	15I	11I	22I	20H	27H	24H
Control[d]		35	26	35	25	36	28	38	27	35	28	37	26

[a] — = no effect, L: low activity = mean of zone diameter ≤ 1/3 of mean zone diameter of control, I: intermediate activity = mean of zone diameter ≤ 2/3 of mean zone diameter of control, H: high activity = mean of zone diameter > 2/3 of mean zone diameter of control. [b] Calculated from 3 values. [c] Identified on the basis of routine cultural, morphological and microscopic characteristics. [d] Chloramphenicol in the case of Gram-positive bacteria, cephalothin in the case of Gram-negative bacteria and cycloheximide in the case of fungi.

© 2022 The Author(s). Published by the Royal Society of Chemistry

Open Access Article. Published on 19 October 2022. Downloaded on 2/8/2026 7:06:59 AM. This article is licensed under a Creative Commons Attribution-NonCommercial 3.0 Unported Licence.

Table 7 Docking data of ligand and its complexes

Compounds	Ligand	Receptor			Interaction		Distance[b]	E^a
Ligand	O7	NZ	LYS	9	(B)	H-Acceptor	2.98	−0.8
	O11	MG	MG	159	(B)	Coordinate	2.37	−1.9
	O14	MG	MG	159	(B)	Coordinate	2.29	−1.7
	6-Ring	ND2	ASN	112	(B)	Pi-H	4.51	−2.4
$[Ni(L)_3](NO_3)_2 \cdot 0.5MeOH$ (**2**)	O28	NZ	LYS	9	(B)	H-Acceptor	2.95	−18.0
	O43	ND2	ASN	112	(B)	H-Acceptor	3.19	−2.1
	6-Ring	NH1	ARG	102	(B)	Pi-cation	3.56	−0.8
$[Ni(L)(Phen)(H_2O)(MeOH)](NO_3)_2$ (**6**)	O30	NE2	HIS	52	(B)	H-Acceptor	2.89	−14.0
	Ni29	MG	MG	159	(B)	Ionic	1.52	−28.5
$[Co(L)_3](NO_3)_2 \cdot MeOH$ (**8**)	O28	NZ	LYS	9	(B)	H-Acceptor	2.97	−18.6
	O43	ND2	ASN	112	(B)	H-Acceptor	3.12	−2.8
$[Co(L)(Phen)(MeOH)_2](NO_3)_2$ (**11**)	O30	NE2	HIS	52	(B)	H-Acceptor	3.40	−1.7
	CO29	MG	MG	159	(B)	Ionic	1.47	−30.3

[a] kcal mol^{-1}. [b] Å

The docking data agreed with the antimicrobial activity data of the ligand and its complexes **2**, **6**, **8** and **11**, where the ligand has the highest antimicrobial activity and formed 4 bonds, while its complexes formed 2 or 3 bonds.

$$\text{Normalized B.S.}^a = 2.69 + 0.0592 \log P - 0.0232 \text{ refractivity} + 0.0628 \text{ polarizability} + 0.481\mu^{**} + 0.289w + 1.44\sigma$$

[a] *Bacillus subtilis* (0.5 mg mL^{-1})/control.$n = 9$, R-sq = 88.5%, SS = (0.067200), MS = (0.009914 + 0.003857) = 0.013771, $F = 2.57$ and $P = 0.306$

$$\text{Normalized C.A.}^b = 0.307 + 0.0339 \log P - 0.0297 \text{ refractivity} + 0.0932 \text{ polarizability} - 0.105\mu^{**} - 0.134w - 0.394\sigma$$

[b] *Candida albicans* (0.5 mg mL^{-1})/control.$n = 9$, R-sq = 87.1%, SS = 0.040249, MS = (0.005845 + 0.002589) = 0.008434, $F = 2.26$ and $P = 0.338$.

3.9. Molecular modeling

Molecular modelling of the optimized compounds (Fig. 7) was carried out using the Hyperchem 7.52 program. The structures were fully optimized and geometric calculations were done to obtain structural parameters such as bond length, atomic charge distributions of the complexes, heat of formation, dipole moment, E_{HOMO}, E_{LUMO}, energy band gaps, and polarizabilities.

The values of E_{HOMO} (eV), E_{LUMO} (eV) and E_{gap} (eV) of the binary complexes (Table 8) that include the acetate anions increase in the following order: Ni(II)- > Co(II)-complexes. Consequently, the band gap values of the complexes are less than that of the free chromone ligand, which means that, in any excitation process, the complexes need less energy than the free ligand. These orders reveal that the stability of the complexes is in the same order of increasing E_{gap}. On the other hand, the E_{gap} values of the binary and ternary chlorides show the order Ni- ≫ Co-complex, but the binary nitrate and ternary complexes of phenanthroline (phen) show the trend Co- > Ni-complex and the stability decreases in the same direction. These differences in the order of E_{gap} might arise from the unlike hard–soft acid–base interactions (HSBA).

The heats of formation of all complexes under study are exothermic. The $[Co(L)_2(OAc)_2]\cdot 1.5H_2O$ complex has the most negative heat of formation (−592.47 kcal mol^{-1}), so it is more thermodynamically stable compared to the other complexes. The complex $[Ni(L)_2Cl_2]$ has the most positive heat of formation and is the least stable.

Global chemical reactivity indices such as total energy, electronic chemical potential (μ), chemical hardness (η), electrophilicity (ω), softness (σ) and dipole moment (μ) are used to describe the reactivity and stability of any chemical compound.

The dipole moment in a molecule is an important property that is mainly used to study intermolecular interactions involving nonbonded type dipole–dipole interactions, because the higher the dipole moment, the stronger the expected intermolecular interactions. Increasing the stability of the complex formation is complemented by increasing the dipole moment value (more polarity) of the complex. Table 8 reveals that the highest polarity complex is $[Co(L)_2(OAc)_2]\cdot 1.5H_2O$ (12.07 Deby), while the least polar complex is $[Co(L)_3](NO_3)_2\cdot MeOH$ (2.61 Deby).

The reactivity of complexes is Co(II)- > Ni(II)-complexes as indicated from the hardness (η) values in Table 8.[43b]

Electronic chemical potential (μ) describes the charge transfer within a system in the ground state. It is defined as the negative of electro-negativity. Physically, the electronic chemical potential (μ) is defined as the tendency of electrons to escape from the equilibrium state. Compounds having greater values of chemical potential are more reactive than those with smaller electronic chemical potential. The data in Table 8 reveals that the capability of an electron to leave the complex molecule based on the chemical potential (μ) values takes the order Ni(II)- > Co(II)-complexes. Therefore, $[Ni(L)_2(OAc)_2]\cdot H_2O$ complex is the strongest electrophile while $[Co(L)(8\text{-HQ})_2]\cdot 1.5H_2O$ is the strongest nucleophile.

The electrophilicity index (ω) measures the stabilization of energy when the system acquires an additional electronic charge from the environment. The data in Table 8 reveal that

© 2022 The Author(s). Published by the Royal Society of Chemistry

Open Access Article. Published on 19 October 2022. Downloaded on 2/8/2026 7:06:59 AM.
This article is licensed under a Creative Commons Attribution-NonCommercial 3.0 Unported Licence.

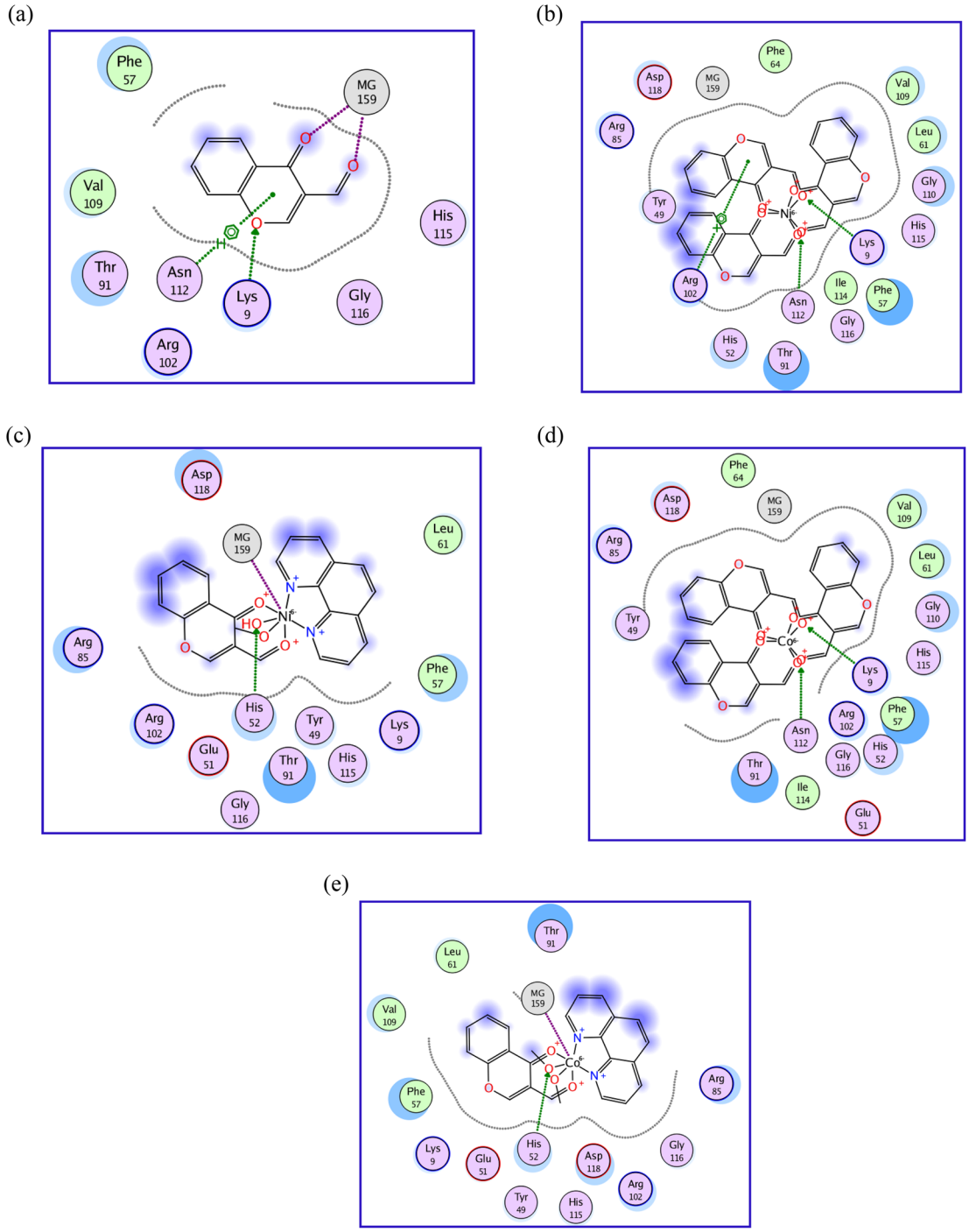

Fig. 6 (a) 2D diagram of ligand interaction with *S. aureus* nucleoside diphosphate kinase, PDB ID: 3Q89. (b) 2D diagram of Ni(II)- complex **2** interaction with *S. aureus* nucleoside diphosphate kinase, PDB ID: 3Q89. (c) 2D diagram of Ni(II)- complex **6** interaction with *S. aureus* nucleoside diphosphate kinase, PDB ID: 3Q89. (d) 2D diagram of Co(II)- complex **8** interaction with *S. aureus* nucleoside diphosphate kinase, PDB ID: 3Q89. (e) 2D diagram of Co(II)- complex **11** interaction with *S. aureus* nucleoside diphosphate kinase, PDB ID: 3Q89.

the most powerful electrophile is the binary $[Co(L)_2Cl_2]$ complex with $\omega = -7.28$ eV, while the weakest electrophile is the binary $[Ni(L)_3](NO_3)_2 \cdot 0.5MeOH$ complex with $\omega = -2.23$ eV. The softness (σ) of the complexes ranges from -0.28 to -1.80 eV^{-1}.

Based on the values in Table 9, it is observed that when these ligands are coordinated with the metal ion, there is an elongation of the bond length between the above-mentioned atoms which confirms the coordination of the carbonyl oxygen with the metal ion. When the atoms are coordinated with the metal ion by donating a lone pair of electrons, there is a decrease in electron density on the coordinating atoms, hence the bond length increases in the metal complexes. A comparison of the bond lengths of the ligand and its metal complexes is demonstrated in Table 9. The bond lengths from the *PM3* method for

Open Access Article. Published on 19 October 2022. Downloaded on 2/8/2026 7:06:59 AM.
This article is licensed under a Creative Commons Attribution-NonCommercial 3.0 Unported Licence.

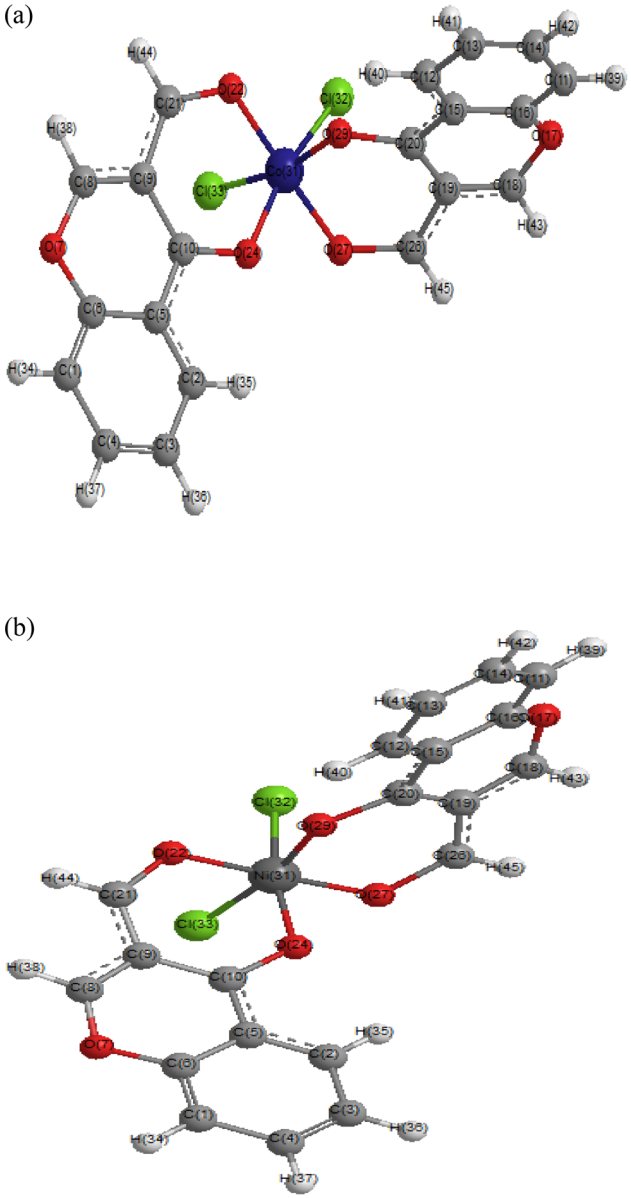

Fig. 7 (a) Optimized structure of $[(L)_2CoCl_2]$ (9) using Hyperchem 7.52 at PM3 level. (b) Optimized structure of $[(L)_2NiCl_2]$ (4) using Hyperchem 7.52 at *PM3* level.

C=O of the chromone after complexation are between 1.23 and 1.50 Å, longer than that of the free ligand (1.21 Å). Moreover, the M–O bond length of the metal ion with the carbonyl group was found to be in the range 1.86–1.97 Å.

The charge densities on the coordinating centres and the central metal ions are tabulated in Table 10. The results show that the range of charge density is lower in the case of Co(II)-complexes (0.011 to −0.142) than the electron density on the central metal ion of Ni(II)-complexes (−0.613 to −0.898).

The data in Table 11 show the following: (i) as ΔH increases, the lengths of C=Oγ pyrone, C=O and ν(M–O) increase, but the lengths of C=Oγ–M pyrone, C=O–M and ν(C=O) decrease. (ii) The positive slope of the relationship between E_{LUMO} and the bond lengths of C=O and C=Oγ pyrone indicates that increasing E_{LUMO} leads to increasing stability and increasing bond lengths of C=O and C=Oγ pyrone. On the other hand, the linear correlation between the calculated E_{HOMO} with the frequency of C=O and M–O indicates that increasing E_{HOMO} leads to an increase in C=O and a decrease in M–O. (iii) However, increasing ΔE_{gab} leads to increasing stability and ν(M–N) and decreasing ν(C=O) and λ_{max}.

Table 12 shows that the QSAR properties of the complexes are higher than those of the ligand, including surface area (420.91–70, 558.50–738.27), octanol–water partition coefficient (lipophilicity, log *P*, −1.84 to −0.04, 0.25–2.53), volume (982.79–1330.37), refractivity (103.68–150.72), polarizability (34.54–49.48) and molecular weight (443.05–581.40). The hydration energy for the ligand (7.40 kcal mol^{-1}) changed to −1.2 to −26.15 kcal mol^{-1} for its complexes.

4. Conclusion

The coordinating behavior of 3-formylchromone towards Ni(II) and Co(II) ions was investigated through the preparation of a series of binary and ternary metal complexes using metal ions with different anions (AcO^-, NO_3^-, ClO_4^- and Cl^-) and secondary ligands including N,O-donor 8-hydroxyquinoline or N,N-donor 1,10-phenanthroline. The prepared complexes were characterized by microanalytical, spectral, thermal, magnetic, and conductivity techniques. The analytical and spectroscopic techniques revealed the following: (i) all complexes exhibited octahedral geometry. (ii)

Table 8 Molecular orbital parameters in detail and global reactivity of the binary and ternary metal complexes of chromone ligand using Hyperchem 7.52 at the *PM3* level

No.	Complex	E_{LUMO}	E_{HOMO}	ΔE_{gab}	Dipole moment	ΔH	T.E complex	η	μ	σ	ω
	Ligand	−0.880	−9.770	8.890	4.080	−63.830	−49 742.0	−4.4500	5.325	−0.22	−3.19
1	$[Ni(L)_2(OAc)_2]\cdot H_2O$	−1.360	−7.528	6.168	8.494	−550.090	−163 798.7	3.0839	−4.44415	−0.32	3.2022
2	$[Ni(L)_3](NO_3)_2\cdot 0.5MeOH$	−0.724	−6.387	5.663	2.627	−380.629	−173 313.0	2.8315	−3.5555	−0.35	2.2323
3	$[Ni(L)_2(H_2O)_2](ClO_4)_2\cdot H_2O$	−0.802	−6.566	5.764	2.677	−444.901	−138 578.4	2.8817	−3.68395	−0.35	2.3548
4	$[Ni(L)_2Cl_2(H_2O)_2]$	−1.527	−6.974	5.447	10.730	−316.125	−138 166.6	2.7236	−4.25045	−0.37	3.3167
5	$[Ni(L)(8\text{-}HQ)_2]\cdot 1.5H_2O$	−0.744	−7.910	7.166	3.730	−190.970	−148 218.6	3.5830	−4.327	−0.28	2.6127
6	$[Ni(L)(Phen)(H_2O)(MeOH)](NO_3)_2$	−1.628	−5.614	3.986	10.700	−299.620	−135 354.6	1.9932	−3.62115	−0.50	3.2894
7	$[Co(L)_2(OAc)_2]\cdot 1.5H_2O$	−2.042	−3.420	1.378	12.070	−592.470	−157 975.3	0.6892	−2.7308	−1.45	5.4101
8	$[Co(L)_3](NO_3)_2\cdot MeOH$	−1.035	−7.514	6.479	2.612	−482.560	−67 549.1	3.2395	−4.2745	−0.31	2.8201
9	$[Co(L)_2Cl_2]$	−2.290	−3.404	1.114	11.270	−417.470	−132 402.1	0.5570	−2.847	−1.80	7.2759
10	$[Co(L)(8\text{-}HQ)_2]\cdot 1.5H_2O$	−1.208	−3.712	2.504	4.733	−373.310	−142 935.1	1.2520	−2.46	−0.80	2.4168
11	$[Co(L)(Phen)(MeOH)_2](NO_3)_2$	−0.783	−6.853	6.070	6.132	−396.250	−133 028.5	3.0352	−3.81795	−0.33	2.4013

© 2022 The Author(s). Published by the Royal Society of Chemistry

Open Access Article. Published on 19 October 2022. Downloaded on 2/8/2026 7:06:59 AM. This article is licensed under a Creative Commons Attribution-NonCommercial 3.0 Unported Licence.

Table 9 Theoretical calculated bond lengths (Å) of the ligand and its metal complexes on the *PM3* level

No.	Compound	C=O	C=Oγ pyrone	M–O=C	M–O=Cγ	Other bond lengths
	L	1.21	1.22	—	—	—
1	$[Ni(L)_2(OAc)_2]\cdot H_2O$	1.23	1.25	1.86	1.86	M-OAC 1.86–1.816
2	$[Ni(L)_3](NO_3)_2\cdot 0.5MeOH$	1.50	1.50	1.88	1.89	—
3	$[Ni(L)_2(H_2O)_2](ClO_4)_2\cdot H_2O$	1.50	1.50	1.876	1.88	M-OH_2 1.88–1.87
4	$[Ni(L)_2Cl_2(H_2O)_2]$	1.50	1.50	1.878	1.88	M-Cl 2.14–2.13
5	$[Ni(L)(8\text{-}HQ)_2]\cdot 1.5H_2O$	1.49	1.50	1.88	1.87	M-8Hq 1.90–1.89
6	$[Ni(L)(Phen)(H_2O)(MeOH)](NO_3)_2$	1.24	1.24	1.92	1.97	M-10Phen, 1.80 M-$OHCH_3$, 1.29 M-OH_2, 2.008
7	$[Co(L)_2(OAc)_2]\cdot 1.5H_2O$	1.29	1.27	1.87	1.94	M-OAC 1.88–1.86
8	$[Co(L)_3](NO_3)_2\cdot MeOH$	1.28	1.28	1.89	1.93	—
9	$[Co(L)_2Cl_2]$	1.25	1.289	1.90	1.91	M-Cl 2.21
10	$[Co(L)(8\text{-}HQ)_2]\cdot 1.5H_2O$	1.29	1.26	1.915	1.94	M-8Hq 1.90
11	$[Co(L)(Phen)(MeOH)_2](NO_3)_2$	1.329	1.34	1.892	1.86	M-10Phen, 1.90 M-$OHCH_3$, 1.993 M-OH_2, 2.023

Table 10 Theoretical calculations of charge density on the coordinating centers of the binary and ternary metal complexes of the ligand using Hyperchem 7.52 at the *PM3* level

No.	Complex	C=O (1)	CHO (1)	C=O (2)	CHO (2)	C=O (3)	CHO (3)	Metal	Other molecules
1	$[Ni(L)_2(OAc)_2]\cdot H_2O$	0.013	−0.016	0.003	−0.013			−0.623	OAc = −0.168 OAc = −0.171
2	$[Ni(L)_3](NO_3)_2\cdot 0.5MeOH$	0.013	−0.034	−0.010	−0.169	−0.001	−0.029	−0.731	
3	$[Ni(L)_2(H_2O)_2](ClO_4)_2\cdot H_2O$	−0.029	−0.004	0.008	−0.034			−0.693	OH_2 = −0.079 OH_2 = −0.091
4	$[Ni(L)_2Cl_2(H_2O)_2]$	0.036	0.003	0.030	0.001			−0.613	Cl = −0.199 Cl = −0.202
5	$[Ni(L)(8\text{-}HQ)_2]\cdot 1.5H_2O$	−0.093	−0.107					−0.856	N-8hy = 0.026 O-8hy = −0.129 N-8hy = 0.944 O-8hy = −0.110
6	$[Ni(L)(Phen)(H_2O)(MeOH)](NO_3)_2$	−0.051	−0.138					−0.898	N-phen = 0.766 N-phen = 0.831 MeOH = −0.210 OH_2 = −0.105
7	$[Co(L)_2(OAc)_2]\cdot 1.5H_2O$	−0.22	−0.199	−0.145	−0.063			0.011	OAc = −0.371 OAc = −0.441
8	$[Co(L)_3](NO_3)_2\cdot MeOH$	−0.209	−0.221	−0.207	−0.222	−0.207	−0.221	−0.012	
9	$[Co(L)_2Cl_2]$	−0.169	−0.050	−0.205	−0.121			−0.042	Cl = −0.424 Cl = −0.330
10	$[Co(L)(8\text{-}HQ)_2]\cdot 1.5H_2O$	−0.193	−0.273					−0.123	O-8hy = −0.270 N-8hy = 0.378 O-8hy = −0.272 N-8hy = 0.42
11	$[Co(L)(Phen)(MeOH)_2](NO_3)_2$	−0.178	−0.237					−0.142	MeOH = −0.225 MeOH = −0.196 N-phen = 0.175 N-phen = 0.171

Open Access Article. Published on 19 October 2022. Downloaded on 2/8/2026 7:06:59 AM. This article is licensed under a Creative Commons Attribution-NonCommercial 3.0 Unported Licence.

Table 11 The correlations between the UV-Vis and IR spectra experimental values and the structural parameters of the complexes

No.	Equation	r%	Complexes
1	$\Delta H = 8584(1327) - 4718(697.0)$ LM–O=Cγ	92.0%	**2, 4, 5, 7, 8 & 9**
2	$\Delta H = 23\,486(5801) - 12\,684(3081)$ LM–O=C	94.4%	**1, 5, 8 & 11**
3	$\Delta H = -2015(216.5) + 1215(159.8)$ LC=Oγ pyrone	96.7%	**5, 8, 9 & 11**
4	$\Delta H = -2246\ (74.06) + 1382(55.44)$ LC=O	99.7%	**1, 5, 8 & 11**
5	$\Delta H = -1723(190.1) + 2.51(0.3557)\ \nu$(M–O)	94.3%	**2, 3, 6, 9 & 10**
6	$\Delta H = 10\,442(933.4) - 6.73(0.5817)\ \nu$(C=O)	97.8%	**2, 3, 5, 10 & 11**
7	$E_{LUMO} = -12.9(2.932) + 9.17(2.281)$ L(C=O)	89.0%	**6, 8, 10 & 11**
8	$E_{LUMO} = -10.7(2.269) + 7.44(1.781)$ L(C=Oγ pyrone)	85.3%	**1, 6, 8, 10 & 11**
9	$E_{HOMO} = -138(17.45) + 0.0812(0.01082)\ \nu$(C=O)	98.3%	**1, 3 & 11**
10	$E_{HOMO} = 27.8(4.786) - 0.0589(0.008783)\ \nu$(M–O)	97.8%	**6, 9 & 10**
11	$\Delta E_{gab} = 8.35(0.4251) - 0.00443(0.0007426)\ \lambda_{max}$	92.2%	**1–4 & 11**
12	$\Delta E_{gab} = -69.2(9.483) + 0.170(0.02178)\ \nu$(M–N)	96.8%	**1–4 & 10**
13	$\Delta E_{gab} = 65.2(7.133) - 0.0367(0.004445)\ \nu$(C=O)	95.8%	**1, 3, 5, 8 & 11**

Table 12 QSAR properties of complexes calculated using Hyperchem 7.52 at the *PM3* level

No.	Compound	Surface area approx.	Surface area grid	Volume	Hydration energy (kcal mol^{-1})	-log *P*	Refractivity	Polarizability	MW
	L	277.25	329.02	508.16	7.40	−0.61	50.43	17.62	174.16
1	$[Ni(L)_2(OAc)_2]\cdot H_2O$	539.52	661.83	1184.05	−5.40	1.15	123.91	42.56	525.11
2	$[Ni(L)_3](NO_3)_2\ \cdot\ 0.5$MeOH	533.21	734.75	1317.94	−2.24	1.89	150.72	49.48	581.18
3	$[Ni(L)_2(H_2O)_2](ClO_4)_2\cdot H_2O$	420.91	558.50	982.79	−26.15	−0.04	103.68	34.54	443.05
4	$[Ni(L)_2Cl_2(H_2O)_2]$	458.21	585.96	1016.94	−2.04	2.53	112.75	37.63	477.93
5	$[Ni(L)(8\text{-HQ})_2]\cdot 1.5H_2O$	476.07	681.64	1214.83	−7.16	0.52	143.98	48.95	521.17
6	$[Ni(L)(Phen)(H_2O)(MeOH)](NO_3)_2$	430.52	611.56	1085.19	−8.78	−1.84	120.70	41.40	463.13
7	$[Co(L)_2(OAc)_2]\cdot 1.5H_2O$	535.92	670.61	1196.48	−4.97	1.15	123.91	42.55	525.33
8	$[Co(L)_3](NO_3)_2\cdot$MeOH	552.44	738.27	1330.37	−1.43	1.89	150.72	49.47	581.40
9	$[Co(L)_2Cl_2]$	514.62	604.21	1044.40	−1.21	2.53	112.75	37.62	478.15
10	$[Co(L)(8\text{-HQ})_2]\cdot 1.5H_2O$	647.70	560.06	1022.02	−2.53	0.25	129.92	41.19	504.26
11	$[Co(L)(Phen)(MeOH)_2](NO_3)_2$	427.16	608.82	1115.62	−4.16	−1.59	125.59	43.23	477.38

The ligand behaves as a neutral bidentate, forming chelates that reflect the non-coordinating or weakly coordinating power of the ClO_4^- and NO_3^- anions as compared to the strongly coordinating power of the AcO^- anion. (iii) The obtained complexes are formed with different molar ratios according to the anion. In the cases of the AcO^-, ClO_4^- and Cl^- anions, 1 : 2 M : L complexes were obtained. In the case of the NO_3^- anion, 1 : 3 M : L complexes were obtained. (iv) Ternary complexes are formed with two metal- : ligand : secondary ligand molar ratios: 1 : 1 : 2 in the case of 8-hydroxyquinoline and 1 : 1 : 2 in the case of 1,10-phenanthroline. The thermodynamic parameters of the metal complexes were calculated by the Coats–Redfern method and standard thermodynamic equations using the TGA curves from the thermal degradation of the solid complexes. Biological activity and molecular modelling showed good agreement, supported by the theoretical and experimental data.

Conflicts of interest

The authors of the article do not have any conflict of interest.

References

1 A. Husain, P. Ach and B. Anupama, *J. Mol. Struct.*, 2022, **1254**, 132341.
2 A. Innasiraj, B. Anandhi, Y. Gnanadeepam, N. Das, F. Paularokiadoss, A. V. Ilavarasi, C. D. Sheela, D. R. Ampasala and T. C. Jeyakumar, *J. Mol. Struct.*, 2022, **1265**, 133450.
3 M. B. Teimouri, Z. B. Savadjani, M. Shiri, R. Bikas and S. Naderi, *Dyes Pigm.*, 2022, **199**, 110106.
4 X. Yun, L. Chen, Y. Lv, Z. Lu, K. Huang and S. Yan, *Green Synth. Catal.*, 2022, DOI: 10.1016/j.gresc.2022.05.002, in press.
5 (*a*) S. B. A. Ghani, P. J. Mugisha, J. C. Wilcox, E. A. M. Gado, E. O. Medu, A. J. Lmb and R. C. D. Brown, *Synth. Commun.*, 2013, **43**, 1549–1556; (*b*) A. Ramesh, B. Srinivas, R. Pawar and A. Ramachandraiah, *J. Mol. Struct.*, 2022, **1255**, 132377.
6 K. M. Khan, N. Ambreen, U. R. Mughal, S. Jalil, S. Perveen and M. I. Choudhary, *Eur. J. Med. Chem.*, 2010, **45**, 4058–4064.
7 P. M. Kris-Etherton, K. D. Hecker, A. Bonanome, S. M. Coval, A. E. Binkoski, K. F. Hilpert, A. E. Griel and T. D. Etherton, *Am. J. Med.*, 2002, **113**, 71–88.
8 (*a*) T. Zhou, Q. Shi, C.-H. Chen, H. Zhu, L. Huang, P. Ho and K.-H. Lee, *Bioorg. Med. Chem.*, 2010, **18**, 6678–6689; (*b*) V. M. Patil, N. Masand, S. Verma and V. Masand, *Chem. Biol. Drug Des.*, 2021, **98**, 943–953; (*c*) N. Balakrishnan, J. Haribabu, M. Dharmasivam, S. Swaminathan and R. Karvembu, *Appl. Organomet. Chem.*, 2022, **36**, e6750; (*d*)

© 2022 The Author(s). Published by the Royal Society of Chemistry

Open Access Article. Published on 19 October 2022. Downloaded on 2/8/2026 7:06:59 AM. This article is licensed under a Creative Commons Attribution-NonCommercial 3.0 Unported Licence.

I. Yousuf and M. Bashir, *Appl. Organomet. Chem.*, 2021, **35**, e6090.

9 (*a*) E. Venkateswararao, V. K. Sharma, M. Manickam, J. Yun and S.-H. Jung, *Bioorg. Med. Chem. Lett.*, 2014, **24**(22), 5256–5259; (*b*) V. C. Patil, *IJPSR*, 2012, **3**(12), 5006–5014; (*c*) A. Gomes, O. Neuwirth, M. Freitas, D. Couto, D. Ribeiro, A. G. P. R. Figueiredo, A. M. S. Silva, R. S. G. R. Seixas, D. C. G. A. Pinto, A. C. Tomé, J. A. S. Cavaleiro, E. Fernandes and J. L. F. C. Lima, *Bioorg. Med. Chem.*, 2009, **17**, 7218–7226; (*d*) J. E. Philip, S. A. Antony, S. J. Eeettinilkunnathil, M. R. P. Kurup and M. P. Velayudhan, *Inorg. Chim. Acta*, 2018, **469**, 87–97; (*e*) P. Kavitha, M. Saritha and K. L. Reddy, *Spectrochim. Acta, Part A*, 2013, **102**, 159–168; (*f*) P. Mucha, A. Skoczyńska, M. Małecka, P. Hikisz and E. Budzisz, *Molecules*, 2021, **26**(16), 4886; (*g*) M. Gaber, K. El-Baradie, N. Elwakiel and S. Hafez, *Appl. Organomet. Chem.*, 2020, **34**(2), e5348; (*h*) C. Chiruta, D. Schubert, R. Dargusch and P. Maher, *J. Med. Chem.*, 2012, **55**, 378–389; (*i*) S. Selvamurugan, R. Ramachandran, P. Vijayan, R. Manikandan, G. Prakash, P. Viswanathamurthi, K. Velmurugan, R. Nandhakumar and A. Endo, *Polyhedron*, 2016, **107**, 57–67.

10 S. Khursheed, S. Tabassum and F. Arjmand, *Polyhedron*, 2022, **214**, 115638.

11 (*a*) A. Z. El-Sonbati, M. A. Diab, A. K. El-Sayed, M. I. Abou-Dobara and A. A. F. Gafer, *Appl. Organomet. Chem.*, 2022, **36**(5), e6651; (*b*) S. A. Sadeek, S. M. Abd El-Hamid, A. A. Mohamed, W. A. Zordok and H. A. El-Sayed, *Appl. Organomet. Chem.*, 2019, **33**, e4889.

12 (*a*) H. F. Abd El-Halim, G. G. Mohamed and M. N. Anwar, *Appl. Organomet. Chem.*, 2018, **32**, e3899; (*b*) R. Neelaeni, S. Vasantha, R. Keerthana, S. Sivakolunthu and T. Angeline, *Asian J. Pharm. Clin. Res.*, 2016, **9**, 277–281.

13 H. L. Mobley and R. P. Hausinger, *Microbiol. Rev.*, 1989, **53**, 85–108.

14 (*a*) D. Li and G.-Q. Zhong, *Sci. World J.*, 2014, **2014**, 641608; (*b*) S. Altürk, D. Avci, B. Z. Kurt, Ö. Tamer, A. Başoğlu, F. Sn̰mez, Y. Atalay and N. Dege, *J. Inorg. Organomet. Polym. Mater.*, 2019, **29**(4), 1265–1279.

15 (*a*) A. Z. El-Sonbati, M. A. Diab and S. M. Morgan, *J. Mol. Liq.*, 2017, **225**, 195–206; (*b*) M. Carcelli, S. Montalbano, D. Rogolino, V. Gandin, F. Miglioli, G. Pelosi and A. Buschini, *Inorg. Chim. Acta*, 2022, **533**, 120779; (*c*) A. Barma, D. Ghosh, P. Karmakar and P. Roy, *J. Mol. Struct.*, 2022, **1250**, 131687.

16 J. Shi, H. Ge, F. Song and S. Guo, *J. Mol. Struct.*, 2022, **1253**, 132263.

17 P. Patil and S. Zangade, *J. Indian Chem. Soc.*, 2022, **99**, 100274.

18 B. Kaya, D. Akyüz, T. Karakurt, O. Şahin, A. Koca and B. Ülküseven, *Appl. Organomet. Chem.*, 2020, **34**, e5930.

19 M. Echabaane, N. Mhadhbi, A. Rouis and H. Naïli, *Optik*, 2022, **256**, 168770.

20 (*a*) S. Selvamurugan, R. Ramachandran, P. Vijayan, R. Manikandan, G. Prakash, P. Viswanathamurthi, K. Velmurugan, R. Nandhakumar and A. Endo, *Polyhedron*, 2016, **107**, 57–67; (*b*) P. Li, M. Niu, M. Hong, S. Cheng and J. Dou, *J. Inorg. Biochem.*, 2014, **137**, 101–108.

21 A. Pui, C. Policar and J. P. Mahy, *Inorg. Chim. Acta*, 2007, **360**, 2139–2144.

22 (*a*) M. Shebl, O. M. I. Adly, A. Taha and N. N. Elabd, *J. Mol. Struct.*, 2017, **1147**, 438–451; (*b*) O. M. I. Adly and H. F. El-Shafiy, *J. Coord. Chem.*, 2019, **72**(2), 218–238; (*c*) M. Shebl, S. M. E Khalil, M. A. A. kishk, D. M. EL-Mekkawi and M. Saif, *Appl. Organomet. Chem.*, 2019, **33**, e5147; (*d*) R. Fouad and O. M. I. Adly, *J. Mol. Struct.*, 2021, **1225**, 129158.

23 G. H. Jeffery, J. Bassett, J. Mendham and R. C. Denney, *Vogel's Textbook of Quantitative Chemical Analysis*, 5th edn, 1989.

24 F. E. Mabbs and D. I. Machin, *Magnetism and Transition Metal Complexes*, Chapman and Hall, London, 1973.

25 A. Nohara, T. Umetani and Y. Sanno, *Tetrahedron*, 1974, **30**, 3553–3561.

26 A. U. Rahman, M. I. Choudhary and W. J. Thomsen, *Bioassay Techniques for Drug Development*, Harwood Academic Publishers, The Netherlands, 2001.

27 K. M. Khan, Z. S. Saify, A. K. Zeesha, M. Ahmed, M. Saeed, M. Schick, H. J. Kohlbau and W. Voelter, *Arzneim. Forsch.*, 2000, **50**, 915–922.

28 *HyperChem version 7.5*, Hypercube, Inc, 2003.

29 (*a*) A. Dziewulska-Kulaczkowska, *J. Therm. Anal. Calorim.*, 2010, **101**(3), 1019–1026; (*b*) Y. Li and Z. Yang, *J. Coord. Chem.*, 2010, **63**, 1960; (*c*) D.-C. Ilies, E. Pahontu, S. Shova, R. Georgescu, N. Stanica, R. Olar, A. Gulea and T. Rosu, *Polyhedron*, 2014, **81**, 123–131; (*d*) S. J. Mohammed, A. M. Sheat, S. A. Abood and O. M. Yahya, *Egypt. J. Chem.*, 2021, **64**(11), 6423–6427; (*e*) K. T. A. Al-Sultani and N. Al-Lami, *Egypt. J. Chem.*, 2021, **64**(6), 2953–2961.

30 E. M. Abdelrhman, B. A. El-Shetary, M. Shebl and O. M. I. Adly, *Appl. Organomet. Chem.*, 2021, **35**, e6183.

31 S. M. E. Khalil, M. Shebl and F. S. Al-Gohani, *Acta Chim. Slov.*, 2010, **57**, 716–725.

32 (*a*) F. Samy, M. Shebl, A. Taha and H. S. Seleem, *Egypt. J. Chem.*, 2022, **65**(7), 85; (*b*) F. Samy, A. Taha, M. Shebl, H. S. Seleem and F. I. Hanafy, *Egypt. J. Chem.*, 2022, DOI: **10.21608/EJCHEM.2022.138025.6079**, in press.

33 N. T. Madhu and P. K. Radhakrichnan, *Synth. React. Inorg. Met.-Org. Chem.*, 2001, **31**, 315–330.

34 M. Shebl, A. A. Saleh, S. M. E. Khalil, M. Dawy and A. A. M. Ali, *Inorg. Nano-Met. Chem.*, 2021, **51**, 195–209.

35 F. Samy and M. Shebl, *Appl. Organomet. Chem.*, 2020, **34**, e5502.

36 (*a*) M. Shebl, O. M. I. Adly, H. F. El-Shafiy, S. M. E. Khalil, A. Taha and M. A. N. Mahdi, *J. Mol. Struct.*, 2017, **1134**, 649–660; (*b*) M. Gaber, N. El-Wakiel, K. El-Baradie and S. Hafez, *J. Iran. Chem. Soc.*, 2019, **16**, 169–182; (*c*) W. H. Mahmoud, R. G. Deghadi, M. M. I. El Desssouky and G. G. Mohamed, *Appl. Organomet. Chem.*, 2019, **33**, e4556; (*d*) F. Samy and M. Shebl, *Appl. Organomet. Chem.*, 2022, **36**(9), e6650.

37 W. J. Geary, *Coord. Chem. Rev.*, 1971, **7**, 81–122.

Open Access Article. Published on 19 October 2022. Downloaded on 2/8/2026 7:06:59 AM.
This article is licensed under a Creative Commons Attribution-NonCommercial 3.0 Unported Licence.

38 F. A. Cotton and G. Wilkinson, *Advanced Inorganic Chemistry. A Comprehensive Text*, John Wiley and Sons, New York, 4th edn, 1986.
39 M. Shebl, *J. Mol. Struct.*, 2017, **1128**, 79–93.
40 (*a*) M. Shebl, *Spectrochim. Acta, Part A*, 2009, **73**, 313–323; (*b*) S. M. E. Khalil, *Synth. React. Inorg. Met.-Org. Chem.*, 2000, **30**, 19; (*c*) N. V. Kulkarni, M. P. Sathisha, S. Budagumpi, G. S. Kurdekar and V. K. Revankar, *J. Coord. Chem.*, 2010, **63**, 1451–1461.
41 (*a*) F. Samy and M. Shebl, *Appl. Organomet. Chem.*, 2022, **36**(5), e6650; (*b*) K. A. R. Salib, S. L. Stefan, S. M. Abu El-Wafa and H. F. El-Shafiy, *Synth. React. Inorg. Met.-Org. Chem.*, 2001, **31**, 895–915.
42 A. W. Coats and J. P. Redfern, *Nat*, 1964, **201**, 68–69.
43 (*a*) F. Samy, A. Taha and F. M. Omar, *Appl. Organomet. Chem.*, 2022, **35**(11), e6375; (*b*) F. Samy and F. M. Omar, *J. Mol. Struct.*, 2020, **1222**, 128910; (*c*) F. Samy, A. A. T. Ramadan, A. Taha and H. S. Seleem, *Asian J. Chem.*, 2016, **28**, 2650–2660.
44 C. R. Vinodkumar, M. K. M. Nair and P. K. Radhakrishnan, *J. Therm. Anal. Calorim.*, 2000, **61**, 143–149.
45 A. H. M. Siddaligaiah and S. G. Naik, *J. Mol. Struct.*, 2002, **582**, 129–136.
46 B. Murukan and K. Mohanan, *J. Enzyme Inhib. Med. Chem.*, 2007, **22**(1), 65–70.
47 E. Pahon□u, M. Proks, S. Shova, G. Lupa□cu, D.-C. Ilie□, □.-F. Bărbuceanu, L.-I. Socea, M. Badea, V. Păunescu, D. Istrati, A. Gulea, D. Drăgănescu and C. E. D. Pîrvu, *Appl. Organomet. Chem.*, 2019, **33**, e5185.
48 M. A. Ibrahim, A. A. A. Emara, A. Taha, O. M. I. Adly, A. I. Nabeel and N. Salah, *Appl. Organomet. Chem.*, 2022, **36**, e6535.

© 2022 The Author(s). Published by the Royal Society of Chemistry